

SPECTRA SELF-SIMILARITY FOR ALMOST MATHIEU OPERATORS

MICHAEL P. LAMOUREUX, JAMES A. MINGO, AND SYDNEY R. PACHMANN

ABSTRACT. We determine numerically the self-similarity maps for spectra of the almost Mathieu operators, a two-dimensional fractal-like structure known as the Hofstadter butterfly. The similarity maps each have a horizontal component determined by certain algebraic maps, and vertical component determined by a Möbius transformation, indexed by a semigroup of the matrix group $GL_2(\mathbb{Z})$. Based on the numerical evidence, we state and prove a continuity result for the similarity maps. We note a connection between the indexing of the similarity maps and Morita equivalence of rotation algebras A_θ , a continuous field of C^* -algebras.

CONTENTS

1. Introduction	2
2. Numerical evidence: Similarity maps	4
3. Numerical evidence: Vertical similarities from $GL_2(\mathbb{Z})$	6
4. Numerical evidence: A symmetry with break	10
5. Generating the $GL_2(\mathbb{Z})$ symmetries	11
6. Horizontal similarity: Interval maps	12
7. Horizontal similarity: Cubic case $1 \mapsto 1/3$	14
8. Horizontal similarity: Quintic case $1/3 \mapsto 1/5$	16
9. Horizontal similarity: Algebraic curves	17
10. The similarity maps: General case	20
11. The similarity maps: Gap labelling	22
12. The similarity maps: Proof of continuity	23
13. Three generators for the butterfly similarities	28
14. Conclusions	29
Acknowledgments	29
References	30
Appendix 1	31
Appendix 2	33
Appendix 3	34

Date: May 7, 2010.

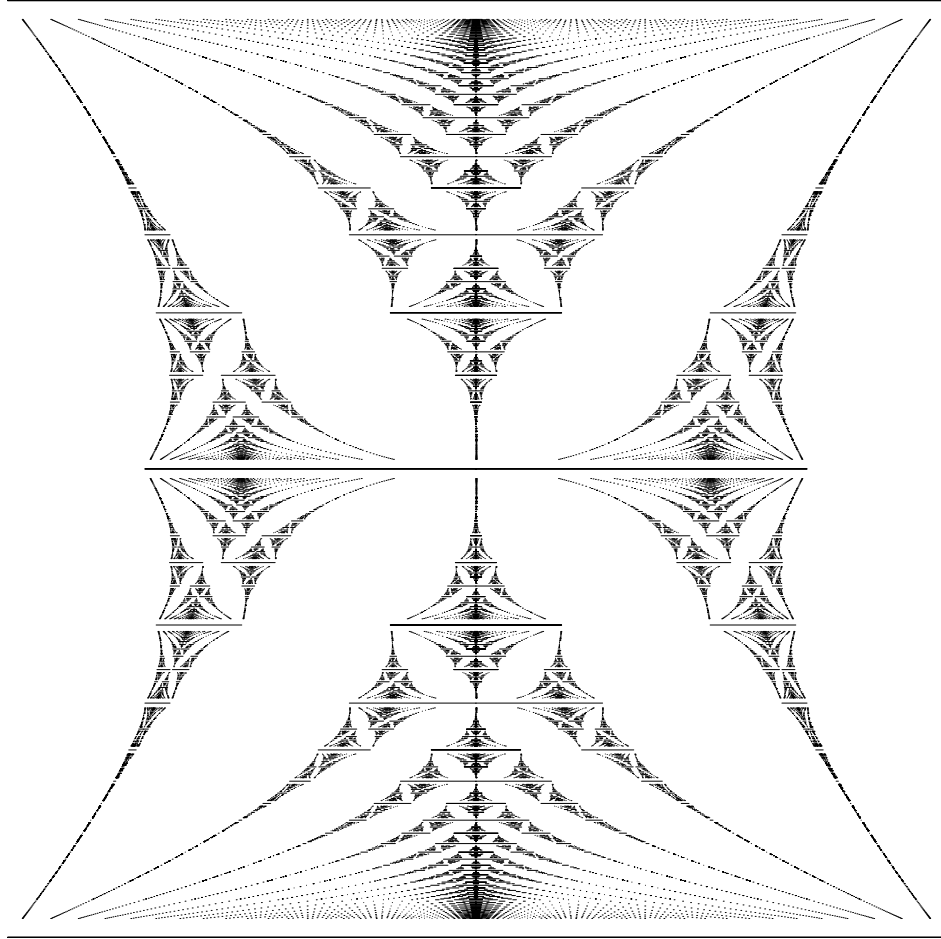


FIGURE 1. The Hofstadter butterfly, a fractal-like structure of line spectra.

1. INTRODUCTION

Looking at the image presented in Figure 1, one immediately notices the striking, repetitive pattern of “butterfly wings” that march off towards the vertical horizons at the top and bottom of the image. This rendering of the so-called Hofstadter butterfly, drawn to high-resolution using a combination of numerical algorithms and PostScript graphics programming, reveals some beautiful symmetries of a fundamentally mathematical object. The goal of this paper is to specify exactly the symmetries of this image and prove continuity results of the corresponding similarity maps, motivated by numerical evidence collected in our study of the butterfly.

Although the Hofstadter butterfly looks like a fractal, the image is not created using the usual iterative equations or recursive graphical methods designed to visually render typical fractals (Mandelbrot, 1990). Rather, this image is created from an explicit numerical computation of spectral values of a family of linear operators on Hilbert space.

More precisely, this image is constructed as a layered suite of horizontal lines which arise as the spectra of almost Mathieu operators. Each of these operators is succinctly represented as the self-adjoint element

$$(1) \quad h_\theta = u + u^* + v + v^*$$

in the C^* -algebra A_θ generated by universal unitaries u, v satisfying the commutation rule

$$(2) \quad vu = e^{2\pi i \theta} uv.$$

In Figure 1, the vertical axis is spanned by the parameter θ , with $0 \leq \theta \leq 1$, while the horizontal axis corresponds to spectral values x in the range $-4 \leq x \leq 4$.

Only rational values of θ are used in the construction of the image in Figure 1. For this reason, the image is properly called the *rational* Hofstadter butterfly. Extensions to irrational values of θ has been a theme in the long history of study these operators and the physical problems that motivated it, going back at least to a mathematical analysis of Bloch electrons (Brown, 1964). A selection of relevant studies over the years is given in the references, including (Avila and Jitomirskaya, 2006; Bellissard and Simon, 1982; Bellissard, 1990; Choi et al., 1990; Connes, 1994; Goldman, 2009; Hofstadter, 1976; Kaminker and Putnam, 2003; Last, 1994; Puig, 2004; Ypma, 2007).

Unlike the irrational case as considered in (Arveson, 1994), rational values of $\theta = p/q$ lead to the computation of spectral lines based on finite dimensional eigenvalue calculations using tridiagonal $q \times q$ matrices (Lamoureux, 1997). In particular, the endpoints of the spectral lines are specified by eigenvalues of these matrices. Numerical algorithms for the tridiagonal eigenvalue computations are rapid and accurate, making calculations of the rational butterfly ideal for numerical experiments. Based on these experiments, we deduce a systematic catalogue of the symmetries of the butterfly.

Repetition of a geometric object fading out to infinity is characteristic of hyperbolic geometry (Coxeter, 1942), hence it is perhaps no surprise that the matrix group $GL_2(\mathbb{Z})$ arises in the observed symmetries. Sections 2 through 5 reveal a semigroup of linear fractional transformations represented by elements of $GL_2(\mathbb{Z})$ which act on the vertical parameter θ to generate the family of similarity maps.

Equally important are the algebraic curves specifying the horizontal component of the similarities, acting on the horizontal parameter x . Sections 6 through 9 present numerical evidence of the continuous maps taking one level of horizontal spectra

to another, using an indexing of intervals and a correspondence of image points under polynomial maps. These are precisely the characteristic polynomials of the aforementioned finite dimensional $q \times q$ matrices giving the spectra.

Uniting the vertical and horizontal components leads to an identification of the general form of the similarity maps, as presented in Section 10. The similarity extends to gap-labelling, a specific method for indexing the butterfly wings based on Chern characters, which is discussed in Section 11. Proof of continuity of the similarity maps is given in Section 12 and generators for the semigroup of similarities is presented in Section 13.

“Xenocides, who is ugly, makes ugly poetry,” said Aristophanes. With the Hofstadter butterfly, we see pretty mathematics making pretty pictures.

2. NUMERICAL EVIDENCE: SIMILARITY MAPS

Mirror image symmetry in the horizontal direction suggests an obvious self-similarity of the image in Figure 1 given by a reflection about the line $x = 0$, namely:

$$(3) \quad (x, \theta) \mapsto (-x, \theta).$$

This map is continuous, and does map the butterfly to itself, as the spectrum of each h_θ is symmetric.

In the vertical direction, another mirror image symmetry in the figure suggests a second self-similarity map given by reflection about the line $\theta = 1/2$, namely:

$$(4) \quad (x, \theta) \mapsto (x, 1 - \theta).$$

Again, this is a continuous map, and again maps spectra properly since the algebra A_θ is isomorphic to $A_{1-\theta}$, with operator h_θ mapping onto $h_{1-\theta}$ under the isomorphism.

Now, a more interesting symmetry is observed mapping the large central butterfly onto the next largest butterfly in the bottom half of the image in Figure 1. Zooming in on this butterfly, as shown in Figure 2, one sees the top of the butterfly at $\theta = 1/3$, the bottom at $\theta = 0$, and the centre of the butterfly at $\theta = 1/4$. This suggest we must find a self-similarity map that, on vertical parameter values θ , will map $\theta \mapsto \theta'$ as

$$(5) \quad 0 \mapsto 0, \quad 1/2 \mapsto 1/4, \quad 1 \mapsto 1/3.$$

No linear map will do, but a linear fractional transformation¹ does work, using the map

$$(6) \quad \theta \mapsto \theta' = \frac{\theta}{2\theta + 1}.$$

¹i.e. a Möbius transformation

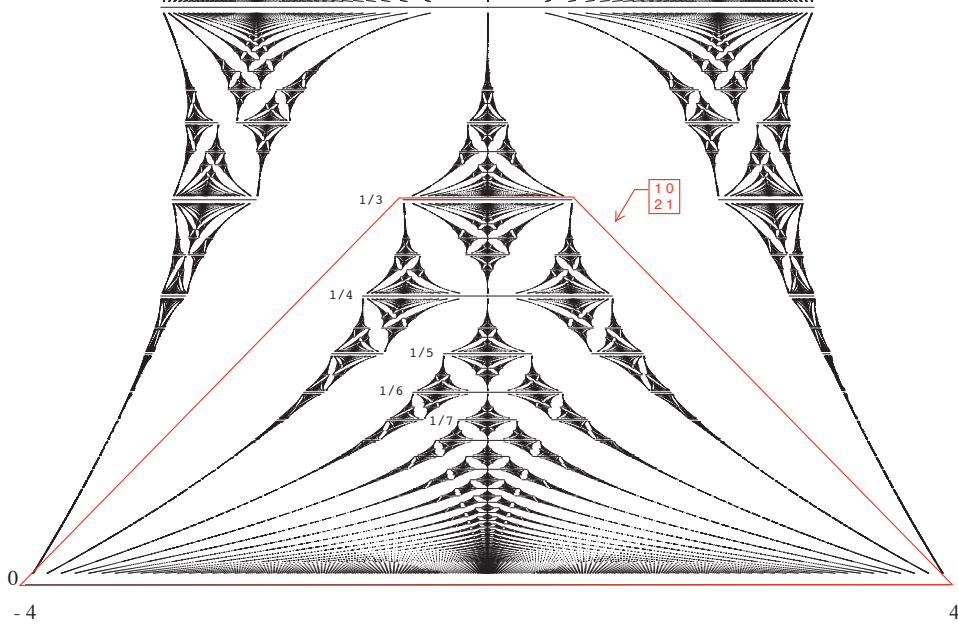


FIGURE 2. Similarity to the bottom third of the butterfly.

It is reassuring to notice that other obvious lines in the full image map correctly under this map. For instance, the line at $\theta = 1/3$ in the full butterfly in Figure 1 should map to the top of the second largest butterfly in Figure 2, which is at $\theta' = 1/5$. And indeed, the LFT here does just that. Similarly we can check for that the line at $1/4$ maps to $1/6$, the line at $1/5$ maps to $1/7$, and so on. Checking numerically many of these lines assures us that the linear fractional transformation is the proper choice.

Going to a numerical experiment based on these observations, we construct a map from the full image in Figure 1 to subset like Figure 2, using the LFT in the vertical component, and contracting linearly in the horizontal component. Specifically, we map according to the rule

$$(7) \quad (x, \theta) \mapsto (x', \theta') = \left((1 - .82 * \theta)x, \frac{\theta}{2\theta + 1} \right).$$

The coefficient 0.82 was chosen to get the correct width for the top horizontal line. The result is the image shown in Figure 3, which is very much like the lower butterfly image in Figure 2.

Observing the slight differences between the image in Figure 1 and the result of the numerical experiment shown in Figure 3, (the difference in the curvature of the

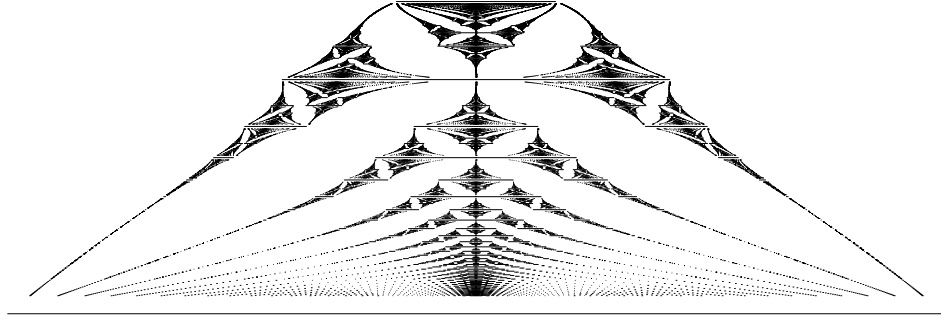


FIGURE 3. A rendering of an approximate similarity to the bottom third, using a linear fractional transformation vertically, linear scaling horizontally.

wingtips for instance), we can conclude the whatever the similarity map is, it is only approximately linear. Nevertheless, the basic structure and position of the tiny butterflies are preserved. This serves as numerical evidence that the vertical maps are indeed given by linear fractional transformations. The horizontal component is more complicated, and is discussed in Sections 7, 8, 9.

3. NUMERICAL EVIDENCE: VERTICAL SIMILARITIES FROM $GL_2(\mathbb{Z})$

Perhaps it is suggestive that two of the self-similarity maps identified so far (vertical flip, and the bottom third map) have vertical components give by Möbius transformations,

$$(8) \quad \theta \mapsto \frac{1-\theta}{1} \text{ and } \theta \mapsto \frac{\theta}{2\theta+1}.$$

Both transformations are specified by a 2×2 matrix in $GL_2(\mathbb{Z})$, in the form

$$(9) \quad M = \begin{bmatrix} a & b \\ c & d \end{bmatrix},$$

yielding a corresponding linear fractional transformation

$$(10) \quad \theta \mapsto \theta' = \frac{a\theta + b}{c\theta + d}.$$

It will be convenient to label these maps by the corresponding matrix, and we note that composition of the LFTs corresponds to matrix multiplication in $GL_2(\mathbb{Z})$.

A leap of faith suggests looking for symmetries in the butterfly indexed by elements of $GL_2(\mathbb{Z})$. Examining Figure 4, we see the bottom of the central core of butterflies, and we can compute a list of matrices that implement the self-similarity map on the

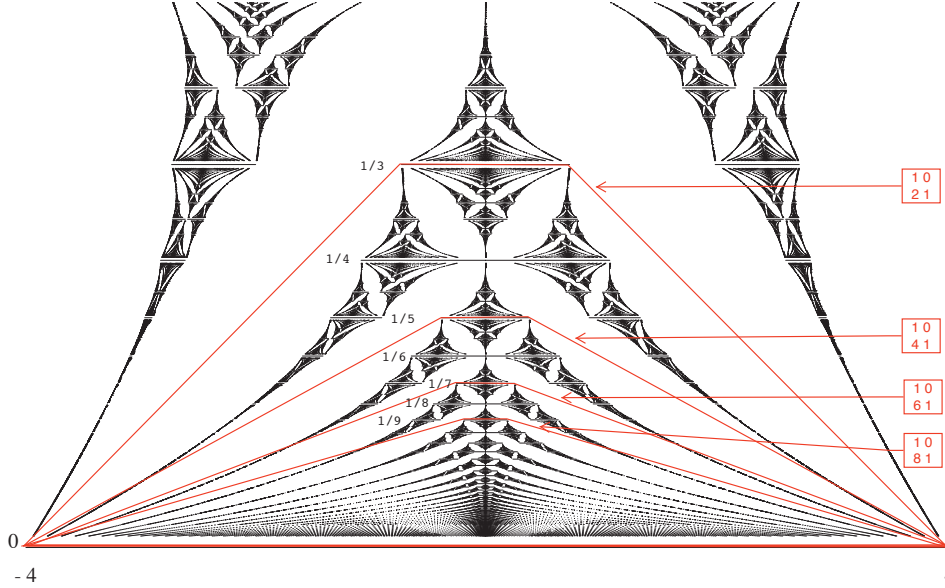


FIGURE 4. A sequence of similarities in the lower central core of the butterfly, and matrices in $SL_2(\mathbb{Z})$ that implement the vertical component of the similarity.

vertical component. For instance, we can map the whole butterfly onto the central bottom butterfly that tops out at label $\theta = 1/5$. For this, we need an LFT that maps $0 \mapsto 0, 1/2 \mapsto 1/6, 1 \mapsto 1/5$. Solving for coefficients a, b, c, d in the LFT, we find the matrix

$$(11) \quad \begin{bmatrix} 1 & 0 \\ 4 & 1 \end{bmatrix}$$

will work to implement an LFT that maps the whole figure into this central bottom butterfly.

Continuing down the central core, we see an infinite sequence of butterflies extending to the “horizon” at $\theta = 0$. Some simple calculations analogous to those above produce a sequence of similarity maps indexed by matrices of the form

$$(12) \quad \begin{bmatrix} 1 & 0 \\ 2n & 1 \end{bmatrix} = \begin{bmatrix} 1 & 0 \\ 1 & 1 \end{bmatrix}^{2n} = A^{2n}, \text{ for } n \geq 1.$$

We will see later that this matrix A is a key generator of the similarities.

Hopping to the top of butterfly, in Figure 5 we see a central core of butterflies extending to the upper “horizon” at level $\theta = 1$. Here, the self-similarity maps are

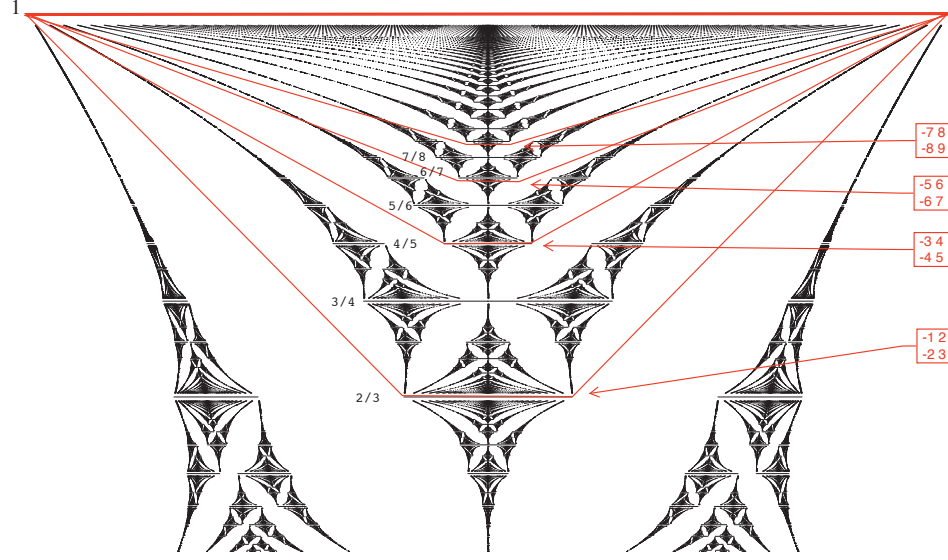


FIGURE 5. A sequence of similarities in the upper central core of the butterfly, and matrices in $GL_2(\mathbb{Z})$ that implement the vertical component of the similarity.

obtained using matrices in $GL_2(\mathbb{Z})$ of the form

$$(13) \quad \begin{bmatrix} 1 - 2n & 2n \\ -2n & 2n + 1 \end{bmatrix}, \text{ for } n \geq 1.$$

Matrices from symmetries on top (Eqn 13) are related to matrices for the symmetries on the bottom (Eqn 12), via the conjugation

$$(14) \quad \begin{bmatrix} 1 - 2n & 1 \\ -2n & 2n + 1 \end{bmatrix} = \begin{bmatrix} -1 & 1 \\ 0 & 1 \end{bmatrix} \begin{bmatrix} 1 & 0 \\ 2n & 1 \end{bmatrix} \begin{bmatrix} -1 & 1 \\ 0 & 1 \end{bmatrix}.$$

This is just conjugation with the flip symmetry map of the butterfly, as the matrix

$$(15) \quad B = \begin{bmatrix} -1 & 1 \\ 0 & 1 \end{bmatrix}$$

induces the linear fractional transformation mapping θ to $1 - \theta$, turning the butterfly upside down.

Attending to some of the butterflies on the side of the image, we find the relevant linear fractional transformations are represented by matrices of the form

$$(16) \quad \begin{bmatrix} 0 & 1 \\ -1 & n \end{bmatrix}, \text{ for } n \leq 3,$$

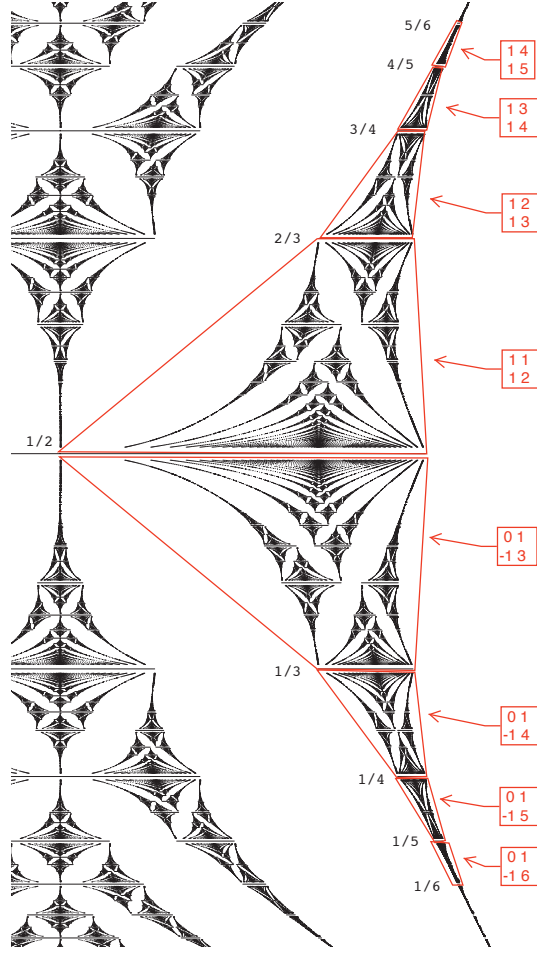


FIGURE 6. A sequence of similarities on the edge of the butterfly, and matrices in $GL_2(\mathbb{Z})$ that implement the similarity.

which generate the symmetries on the bottom half of the image shown in Figure 6. On the top of the image, we obtain transformations indexed by matrices of the form

$$(17) \quad \begin{bmatrix} 1 & n-2 \\ 1 & n-1 \end{bmatrix}, \text{ for } n \geq 3.$$

Again, we observe there is a relation between these two forms of transformation, through conjugation with the flip, as we have

$$(18) \quad \begin{bmatrix} 1 & n-2 \\ 1 & n-1 \end{bmatrix} = \begin{bmatrix} -1 & 1 \\ 0 & 1 \end{bmatrix} \begin{bmatrix} 0 & 1 \\ -1 & n \end{bmatrix} \begin{bmatrix} -1 & 1 \\ 0 & 1 \end{bmatrix}.$$

Note, however, that these self-similarity maps have a certain discontinuity. In particular, the centre of the large butterfly gets mapped to a “broken” butterfly on these side maps. This tells us the self-symmetry maps need not be continuous. In particular there may be a discontinuity in the horizontal direction as we cross the $x = 0$ spectral value.

Nevertheless, this is a mild discontinuity and is easy to understand. In the construction of the Hofstadter butterfly, for $\theta = p/q$ with q even, the spectrum consists of q intervals on the real line, two of which touch at the point zero. (Choi et al., 1990) It is these “touching intervals” that are getting broken apart in the above similarity maps. So although there is an apparent discontinuity, it is perhaps better to describe it as the breaking apart of two touching spectral lines. The similarity map should take the single, common endpoint, and map it to two distinct endpoints of two non-overlapping intervals. The details of this double-valued map will be discussed in Section 10.

4. NUMERICAL EVIDENCE: A SYMMETRY WITH BREAK

As noted in the previous section, under the similarity map sometimes the butterfly breaks. This suggests we can look for more similarities if we are a bit more open to what a broken butterfly looks like.

In Figure 7, we have an example of a really broken butterfly. The butterfly fits into the region

$$(19) \quad 0 \leq \theta \leq 1/2,$$

and the similarity map is given by the linear fractional transformation with matrix

$$(20) \quad \begin{bmatrix} 1 & 0 \\ 1 & 1 \end{bmatrix}.$$

This break (at $\theta = 1/3$) looks pretty bad, but in fact we know from gap labelling theorems that when one plots the gaps an inverse slope 2, there is a discontinuity exactly at $\theta = 1/3$ (Lamoureux, 2010). So in fact this is just confirming the fact that the butterflies are coming from gap labelling.

By including this symmetry, we include the matrix

$$(21) \quad A = \begin{bmatrix} 1 & 0 \\ 1 & 1 \end{bmatrix}$$

in our collection of matrices in $GL_2(\mathbb{Z})$ generating similarity maps.

We observe that all the LFTs seen so far map the θ interval $[0, 1]$ into itself, and are indexed by certain elements of $GL_2(\mathbb{Z})$. This evidence suggests a certain semigroup in $GL_2(\mathbb{Z})$ specifies the possible self-similarity maps. A precise statement identifying the semigroup is given in the next section.

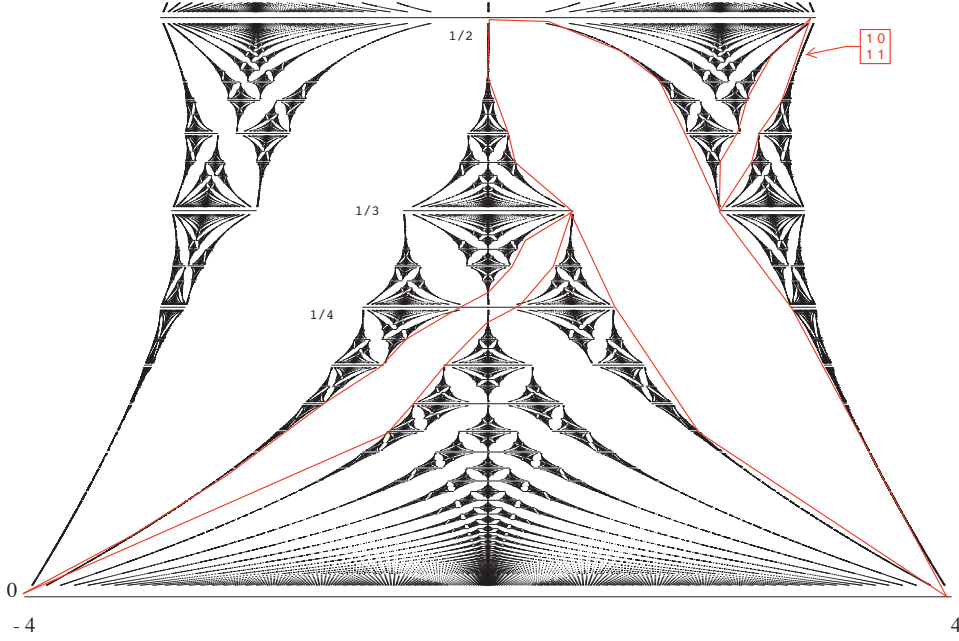


FIGURE 7. An unusual, cracked similarity. Note the basic butterfly structure spanning the bottom half of the full image.

5. GENERATING THE $GL_2(\mathbb{Z})$ SYMMETRIES

The following technical result states that the set of linear fractional transformations which map the interval $[0, 1]$ into itself forms a semigroup, indexed by a 2-generated semigroup of matrices in $GL_2(\mathbb{Z})$.

Theorem 1. *Let G be the semigroup of linear fractional transformations of the form*

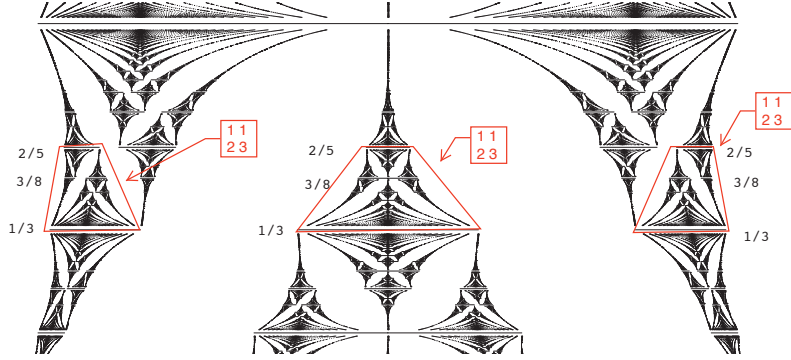
$$(22) \quad \theta \mapsto \theta' = \frac{a\theta + b}{c\theta + d}, \quad \text{for some } \begin{bmatrix} a & b \\ c & d \end{bmatrix} \in GL_2(\mathbb{Z})/\{\pm I\},$$

which map the interval $[0, 1]$ into itself. Then G is generated by the two maps $\phi(\theta) = \theta/(\theta + 1)$ and $\psi(\theta) = 1 - \theta$, represented by matrices

$$(23) \quad A = \begin{bmatrix} 1 & 0 \\ 1 & 1 \end{bmatrix}, \text{ and } B = \begin{bmatrix} -1 & 1 \\ 0 & 1 \end{bmatrix}.$$

The proof of this technical result is given in Appendix 1, and is based on the Euclidean algorithm. We make a few observations about this theorem.

The LFTs do not notice a change of sign in the representing matrix, so the theorem refers to the quotient group $GL_2(\mathbb{Z})/\{\pm I\}$.

FIGURE 8. Multiple similarities, indexed by the same matrix in $SL_2(\mathbb{Z})$.

These two generators correspond to two symmetries for the Hofstadter butterfly. The first generates the map that takes the butterfly to its lower half, mentioned in Section 4. The second is the vertical flip symmetry, mentioned in Section 2. By including the vertical flip in our symmetries, we are able to generate all (vertical components) of the symmetries using only two generating maps.

The fact that the Euclidean algorithm is involved suggests that determining the details of a symmetry map will be rather involved – the factorization into generators is not simple.

It is worth mentioning a deep result from C*-algebras, that states two rotation algebras $A_\theta, A_{\theta'}$ are Morita equivalent if and only if there is a linear fractional transformation mapping

$$(24) \quad \theta \mapsto \theta' = \frac{a\theta + b}{c\theta + d},$$

for some matrix $\begin{bmatrix} a & b \\ c & d \end{bmatrix}$ in $GL_2(\mathbb{Z})$ (Effros and Shen, 1980). We have no idea what connection this might have with the self-similarity maps we have above, which act on spectra of operators in the algebras $A_\theta, A_{\theta'}$, not on the algebras themselves.

6. HORIZONTAL SIMILARITY: INTERVAL MAPS

Considering now the horizontal component of the similarity maps, a close examination of the apparent symmetries suggests the intervals I_1, I_2, \dots, I_q in the spectrum at level $\theta = p/q$ are mapped onto a subcollection of the intervals $I'_1, I'_2, \dots, I'_{q'}$ in the spectrum at level $\theta' = p'/q'$. We note here which subcollections appear.

Examining Figure 8, notice for the single vertical map with linear fractional transformation given by matrix

$$(25) \quad \begin{bmatrix} 1 & 1 \\ 2 & 3 \end{bmatrix},$$

there are in fact three choices of horizontal maps. Start first at initial $\theta = 1$, which maps to $\theta' = 2/5$ under this LFT. The spectrum at level $\theta = 1$ has one interval, while at level $\theta' = 2/5$, there are five intervals that we can map to. Only three are obtained. In the left part of the image in Figure 8, the initial interval I_1 maps onto interval I'_1 ; the middle image maps onto interval I'_3 , and the right image maps onto interval I'_5 . Writing $p'/q' = 2/5$, we see that the three interval maps are given as

$$(26) \quad I_1 \mapsto I'_1 = I'_{0p'+1}, \quad I_1 \mapsto I'_3 = I'_{1p'+1}, \quad I_1 \mapsto I'_5 = I'_{2p'+1}.$$

Checking now at the level $\theta = 1/2$ mapping to $\theta' = 3/8$, the two intervals I_1, I_2 at $\theta = 1/2$ map to two interval I'_1, I'_2 on the left; to the two interval I'_4, I'_5 in the middle; and I'_7, I'_8 on the right. In this case, we have $p'/q' = 3/8$ and we can summarize the left, middle and right maps as

$$(27) \quad I_k \mapsto I'_{0p'+k}, \quad I_k \mapsto I'_{1p'+k}, \quad I_k \mapsto I'_{2p'+k},$$

for $k = 1, 2$. Similarly, at level $\theta = 0$, the single interval I_1 maps as

$$(28) \quad I_1 \mapsto I'_1 = I'_{0p'+1}, \quad I_1 \mapsto I'_3 = I'_{1p'+1}, \quad I_1 \mapsto I'_5 = I'_{2p'+1},$$

where $p'/q' = 1/3$. The form of the interval map is very consistent.

We go back and check the other similarity maps. In Figure 4, the interval maps are apparently of the form

$$(29) \quad I_k \mapsto I'_{n \cdot p + k} = I'_{n \cdot p' + k},$$

for the vertical similarity given by

$$(30) \quad \begin{bmatrix} 1 & 0 \\ 2n & 1 \end{bmatrix}.$$

We can see this by observing the q intervals at level $\theta = p/q$ map to the central q intervals of the set of $q' = 2np + q$ intervals at level $\theta' = p'/q$.

In Figure 5, the interval maps are of the form

$$(31) \quad I_k \mapsto I'_{n \cdot (q-p) + k} = I'_{n \cdot (q'-p') + k},$$

for the vertical similarity given by

$$(32) \quad \begin{bmatrix} 1 - 2n & 2n \\ -2n & 2n + 1 \end{bmatrix}.$$

Again, the q intervals at level $\theta = p/q$ map to the central q intervals of the set of $q' = 2n(q - p) + q$ intervals at level $\theta' = p'/q$.

In Figure 6, a similarity in the top half, say with matrix

$$(33) \quad \begin{bmatrix} 1 & 1 \\ 1 & 2 \end{bmatrix},$$

gives interval maps of the form

$$(34) \quad I_k \mapsto I'_{r \cdot p' + k},$$

with $r = 1$ on the right side of the butterfly (as illustrated), and $r = 0$ on the left side of the butterfly (not shown in Figure 6). However, a similarity in the bottom half of Figure 6, such as with matrix

$$(35) \quad \begin{bmatrix} 0 & 1 \\ -1 & 3 \end{bmatrix},$$

gives interval maps of the form

$$(36) \quad I_k \mapsto I'_{r \cdot (q' - p') + k},$$

with $r = 1$ on the right map, $r = 0$ on the left map.

Generally speaking, it appears there are two types of interval maps, those of the form

$$(37) \quad I_k \mapsto I'_{r \cdot p' + k},$$

and those of the form

$$(38) \quad I_k \mapsto I'_{r \cdot (q' - p') + k},$$

for some choices of non-negative integer r .

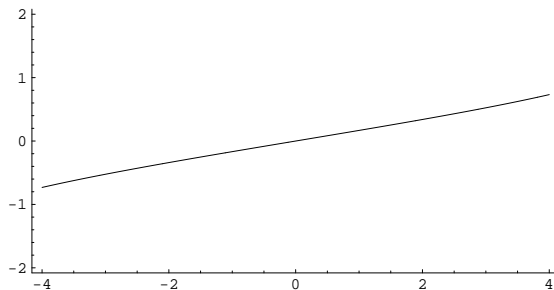
In the next three sections we determine how the horizontal component of the similarity map behaves within each interval I_k .

7. HORIZONTAL SIMILARITY: CUBIC CASE $1 \mapsto 1/3$

The vertical component of the self-similarity map is given by linear fractional transformations, as described in Sections 2 through 4. The horizontal component maps intervals to intervals in the spectra, and appears to be nearly linear, as we saw in the construction of Figure 3. We investigate the details of this horizontal map.

Again referring to the butterfly list in Figure 1, we see that the spectral line at height $\theta = 1$ is approached by a dense cluster of spectral points at heights $\theta < 1$. Under the LFT mapping $\theta \mapsto \theta' = \theta/(2\theta + 1)$, the point $\theta = 1$ maps to $\theta' = 1/3$, and this dense cluster of spectral points near 1 maps to a dense cluster near $1/3$.

We would expect by continuity arguments that the horizontal map at $\theta = 1$ should be well-approximated by following how the nearby cluster points map. Setting rational $p/q = \theta < 1$, we have $p \approx q$, and under the LFT we have $p'/q' = p/(2 * p + q)$.

FIGURE 9. Map from $\theta = 1$ line to $1/3$ lines (middle interval).

There are q points near line 1, and they map to the middle third of the $2p + q \approx 3q$ points under the LFT.

So we do a numerical experiment: Map these cluster points near 1 to corresponding points near $1/3$, and plot the result, to obtain Figure 9. We note the curve is almost linear, but not quite. Performing a best fit polynomial approximation², we find the map is in fact given by

$$(39) \quad x = 6y - y^3.$$

We observe that these polynomial maps are known from earlier work (Choi et al., 1990) as characteristic polynomials P_θ for matrices used to compute the spectra of $q \times q$ matrices representing the operators h_θ in the rotation algebra A_θ , with $\theta = p/q$. Thus, the map we observe is simply

$$(40) \quad P_1(x) = -P_{1/3}(y),$$

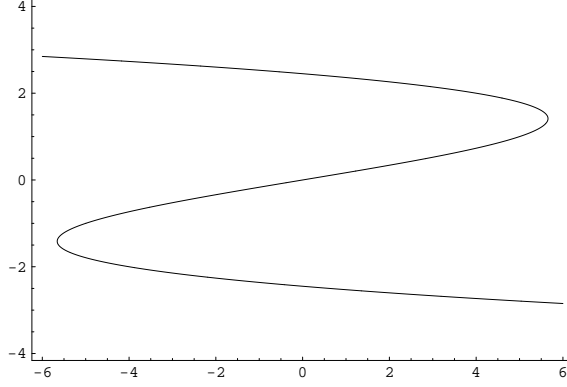
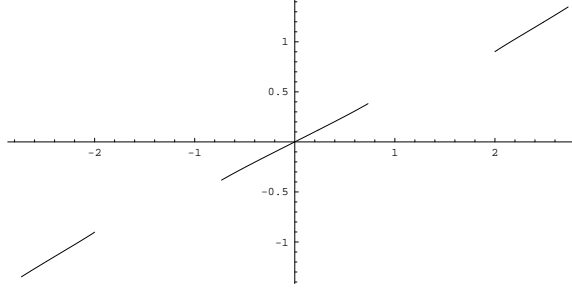
where by $P_{p/q}(x)$ we mean the q -th order characteristic polynomial of the $q \times q$ matrix

$$(41) \quad H = U + U^* + V + V^*,$$

with U the cyclic permutation matrix and V a diagonal matrix with consecutive powers of $e^{2\pi ip/q}$ on the diagonal. Details are in (Choi et al., 1990; Lamoureux and Mingo, 2007).

To see the full algebraic curve, we plot the full curve in Figure 10. Observe the central portion of the curve corresponds to the nearly linear section we saw in Figure 9.

²In fact, in our first numerical experiments, we inadvertently computed the inverse of a polynomial, with expansion $y = x/6 + x^3/1296 + x^5/93312 + \dots$. The second author recognized this as the inverse of a cubic!

FIGURE 10. Algebraic curve $P_1(x) = -P_{1/3}(y)$ defines the 1 to $1/3$ map.FIGURE 11. Map from $1/3$ lines to $1/5$ lines (3 middle intervals).

8. HORIZONTAL SIMILARITY: QUINTIC CASE $1/3 \mapsto 1/5$

We repeat the numerical calculation, using the same central symmetry with LFT given by the matrix

$$(42) \quad \begin{bmatrix} 1 & 0 \\ 2 & 1 \end{bmatrix}.$$

But now we look how the three spectral lines at $\theta = 1/3$ maps to the three central spectral lines at level $\theta' = 1/5$. A numerical experiment as in the last section produces the plot in Figure 11. Again, the three segments look nearly linear, but not quite. An inspired guess suggest these segments come from a portion of the algebraic curve

$$(43) \quad P_{1/3}(x) = -P_{1/5}(y),$$

and a comparison of the two plots shows this is indeed the case.

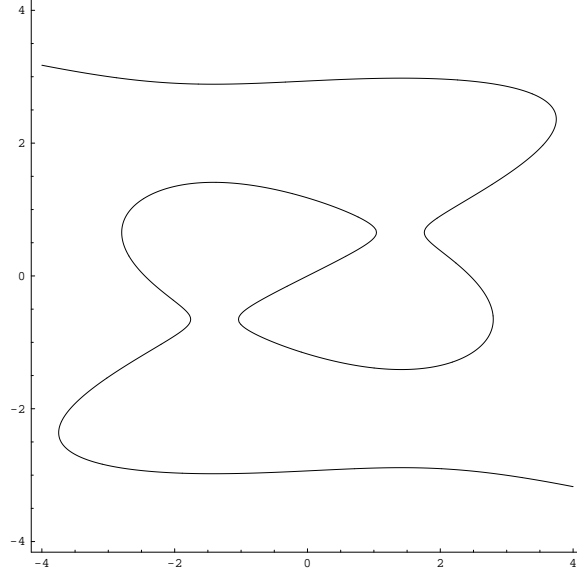


FIGURE 12. Algebraic curve $P_{1/3}(x) = -P_{1/5}(y)$ defines the $1/3$ to $1/5$ map. Note the three nearly linear segments across the centre diagonal, matching Figure 11.

It is worth noting that we can restrict the algebraic curve to the segments shown in Figure 12 by plotting only those points (x, y) such that $P_{1/3}(x) = -P_{1/5}(y)$ and $|P_{1/3}(x)| \leq 4$.

9. HORIZONTAL SIMILARITY: ALGEBRAIC CURVES

We have seen in Sections 7 and 8 that the horizontal maps appear as nearly linear sections of algebraic curves, in the form

$$|P_\theta(x) = \pm P_{\theta'}(x')| \leq 4,$$

for the two characteristic polynomials P_θ and $P_{\theta'}$, where θ, θ' are rational. The full algebraic curves are interesting in themselves, so in this section we present a few plots of the curves and point out some obvious patterns.

Referring to Figure 13, we see the algebraic curves $P_\theta(x) = P_{\theta'}(y)$ for rationals $\theta = 1/q \mapsto \theta' = 1/(q+2)$, with q odd, have a particularly simple graphs. There is a single connected component, that spirals around the origin, with more spirals as the denominator q increases. We see q nearly linear segments, which are the parts of the graph that define the relevant horizontal map on the fractal. We also see the odd symmetries of the curves, that point (x, y) is in the curve if and only if $(-x, -y)$ is in it too.

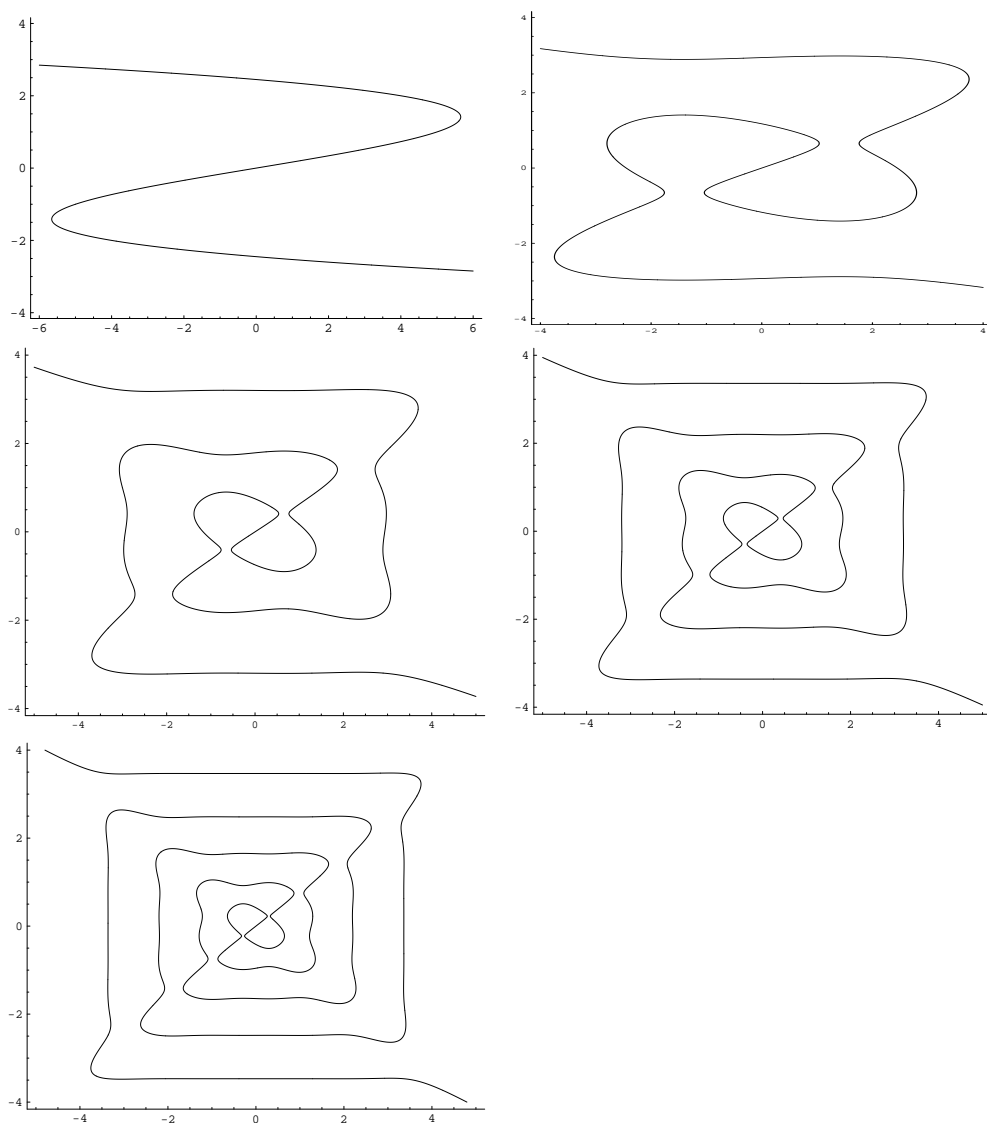


FIGURE 13. A sequence of related algebraic curves, for rationals: $1 \mapsto 1/3$, $1/3 \mapsto 1/5$, $1/5 \mapsto 1/7$, $1/7 \mapsto 1/9$, $1/9 \mapsto 1/11$. Notice the odd number of nearly linear segments down the diagonal of each map.

Referring to Figure 14, we see the maps for rationals $1/q \mapsto 1/(q+2)$, with q even, have somewhat more complex graphs. There are $q/2$ connected components, that form something like figure eights around the origin, with more figure eights as the denominator q increases. We see q nearly linear segments, which are the parts of the

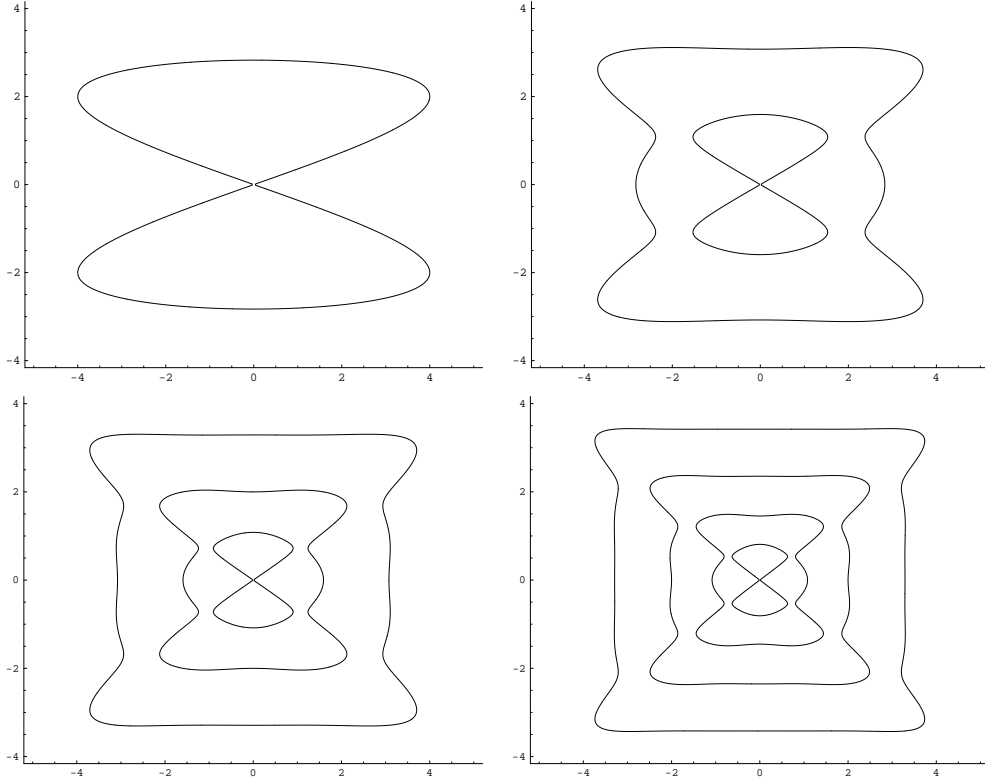


FIGURE 14. A sequence of related algebraic curves: $1/2 \mapsto 1/4$, $1/4 \mapsto 1/6$, $1/6 \mapsto 1/8$, $1/8 \mapsto 1/10$. Notice the symmetry, and the even number of nearly linear segments down the diagonal of each map.

graph that define the relevant horizontal map on the fractal. We also see the even symmetries of the curves, that point (x, y) is in the curve if and only if the points $(\pm x, \pm y)$ are in it too.

Figure 15 examines the curves for rational θ of the form $\theta = p/3$. In both cases ($p = 1/3, 2/3$), there is odd symmetry, there are three nearly linear segments, and some spiraling of the curve about the origin. But for the case $\theta = 2/3$, there are also two additional disconnected components to the curve, that seem to have nothing to do with the linear segments that are involved in the fractal map.

In Appendix 3, we include more plots of these algebraic curves. We note with even denominator q , we have even symmetry in the plots, there are q nearly linear segments, and we see nested “figure eights” defining the key parts of the curve. For $p > 1$, there are disconnected components of the curve that seem to have nothing to do with the main part of the curve that defines the fractal map.

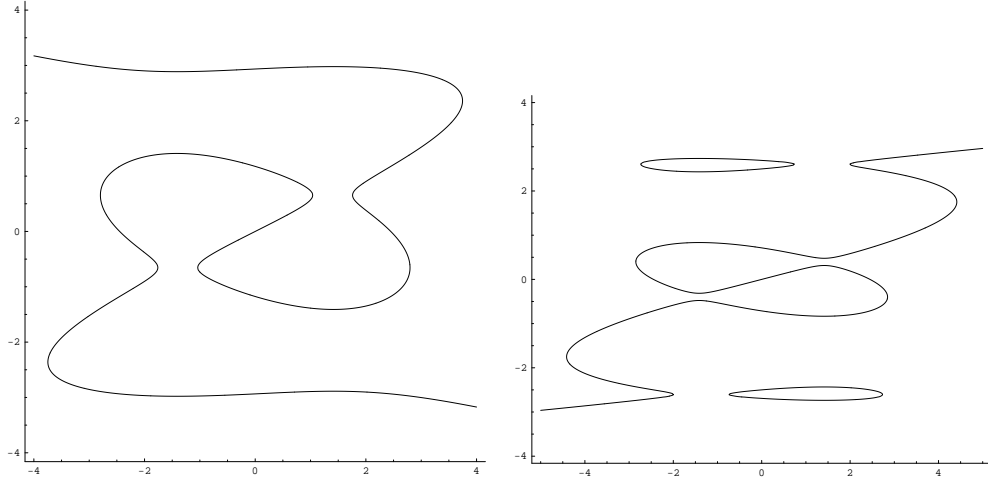


FIGURE 15. Algebraic curves with denominator 3: $1/3 \mapsto 1/5$, $2/3 \mapsto 2/7$. Notice the the three nearly linear segments down the diagonal of each map, and the disconnected components on the right graph.

We also observe the curves appear to get much more complex with increases in the numerator p , for the parameter $\theta = p/q$. There may be some connection between the various straight line segments in curves of different $\theta = p/q$ with the same denominator q , but these patterns are not entirely clear.

We leave discussion of these curves and their connection with symmetries to future work.

10. THE SIMILARITY MAPS: GENERAL CASE

The work in Sections 7 through 9 suggests an obvious candidate for the horizontal maps within spectral intervals: namely, a correspondence of points determined by two characteristic polynomials. Combining this observation with the earlier sections discussing the vertical maps and interval mapping, we can now specify the form of the general similarity maps of the butterfly, as follows:

Fix a matrix element M in $GL_2(\mathbb{Z})$, represented as

$$(44) \quad M = \begin{bmatrix} a & b \\ c & d \end{bmatrix}.$$

Fix an integer $r \geq 0$. The similarity map $S = S_{M,r,+}$ on the rational butterfly is described as

$$(45) \quad (x, \theta) \mapsto S(x, \theta) = (x', \theta'),$$

where the vertical component of the map is given by

$$(46) \quad \theta \mapsto \theta' = \frac{a\theta + b}{c\theta + d},$$

while the horizontal component is given by the interval and polynomial correspondences. Specifically, recall the spectrum at level $\theta = p/q$ is a set of q intervals I_k , $k = 1 \dots q$, while at level $\theta' = p'/q'$ there are q' intervals $I'_{k'}$, $k' = 1 \dots q'$. The map from x at level θ to x' at level θ' is determined by the interval and polynomial conditions

$$(47) \quad x \in I_k \mapsto x' \in I'_{r \cdot p' + k} = I'_{k'} \text{ with } (-1)^{q+k} P_\theta(x) = (-1)^{q'+k'} P_{\theta'}(x').$$

The sign choice for the polynomials is made so that $\pm P_\theta(x)$ and $\pm P_{\theta'}(x')$ are both monotonically increasing on $I_k, I'_{k'}$, respectively. These two conditions determine the image point x' uniquely, except possibly in one special case. Except for this case (described next), we have determined the similarity maps precisely.

The special case to consider is when $x = 0, \theta = p/q$ with q even. In this case, the two intervals $I_{q/2}, I_{q/2+1}$ overlap at $x = 0$ and may map to two disjoint intervals $I'_{k'}$ and $I'_{k'+1}$. Here, we must decide where the point $x = 0$ maps to, either an endpoint of $I'_{k'}$ or to an endpoint of $I'_{k'+1}$. It is convenient to chose to map to *both* points, making the function S double-valued at this point ($x = 0, \theta = p/q$). We will see in the next section that the double-valued function is continuous.

There is another set of similarity maps, $S = S_{M,r,-}$, which differs from the above example by the way the interval maps are selected. For this maps, we chose

$$(48) \quad x \in I_k \mapsto x' \in I'_{r \cdot (q' - p') + k} = I'_{k'},$$

which we observed in Section 6 as similarities that can occur.

Of course, not all such maps $S_{M,r,\pm}$ necessarily appear as similarities of the rational butterfly. For instance, from Theorem 1, we know the matrix M must be chosen from the semigroup $G \subset GL_2(\mathbb{Z})/\pm I$ described in Theorem 1. The integer r must be small enough that

$$(49) \quad r \cdot p' + q \leq q'$$

in the “+” case, and

$$(50) \quad r \cdot (q' - p') + q \leq q'$$

in the “−” case, for all $\theta = p/q$. Equivalently, we have

$$(51) \quad r \leq \min_{\theta} \frac{c\theta + d - 1}{a\theta + b}$$

in the “+” case, and

$$(52) \quad r \leq \min_{\theta} \frac{c\theta + d - 1}{(c - a)\theta + d - b}$$

in the “ $-$ ” case. But these are the only apparent restrictions on M, r, \pm .

11. THE SIMILARITY MAPS: GAP LABELLING

The spectral gaps forming the butterfly are conveniently labeled using a Diophantine equation, where integer parameters (s, t) are fixed, and the k -th gap in the spectrum $\theta = p/q$ is identified using the formula

$$(53) \quad k = t * p - s * q.$$

This indexing is known as gap labelling, as described in (Bellissard, 1990; Goldman, 2009; Kaminker and Putnam, 2003; Ypma, 2007), where the parameters (s, t) are related to Chern numbers. These parameters give a convenient way of labelling the “wings” in the butterfly. Note there is a limited range on the indices: for $t > 0$ we require

$$(54) \quad 0 \leq s \leq t - 1,$$

while for $t < 0$ we require

$$(55) \quad t \leq s \leq -1.$$

It is easy to check that the similarity map $S = S_{M,r,\pm}$ maps labeled gaps to gaps, as stated in the following:

Theorem 2. *The similarity map $S = S_{M,r,+}$ maps the gap labeled (s, t) to the gap (s', t') according to the formula*

$$(56) \quad \begin{bmatrix} s' \\ t' \end{bmatrix} = (ad - bc) \begin{bmatrix} a & b \\ c & d \end{bmatrix} \begin{bmatrix} s \\ t \end{bmatrix} + \begin{bmatrix} 0 \\ r \end{bmatrix}.$$

Also, the similarity map $S = S_{M,r,-}$ maps the gap labeled (s, t) to the gap (s', t') according to the formula

$$(57) \quad \begin{bmatrix} s' \\ t' \end{bmatrix} = (ad - bc) \begin{bmatrix} a & b \\ c & d \end{bmatrix} \begin{bmatrix} s \\ t \end{bmatrix} + \begin{bmatrix} r \\ r \end{bmatrix}.$$

Proof: We consider $S = S_{M,r,+}$. Note the matrix M in the similarity determines the map from angle $\theta = p/q$ to $\theta' = p'/q'$ according to the matrix formula

$$(58) \quad \begin{bmatrix} p' \\ q' \end{bmatrix} = \begin{bmatrix} a & b \\ c & d \end{bmatrix} \begin{bmatrix} p \\ q \end{bmatrix}.$$

In the case where the determinant $ad - bc$ is one, we invert to find

$$(59) \quad p = (dp' - bq') \text{ and } q = (-cp' + aq').$$

The index r of the similarity tells us how intervals I_k are mapped to intervals $I_{k'}$, where $k' = r \cdot p' + k$. Thus the k -th gap is mapped to gap $k' = r \cdot p' + k$. With gap $k = t * p - s * q$, we write

$$\begin{aligned}
 (60) \quad k' &= r \cdot p' + k \\
 (61) \quad &= r \cdot p' + t * p - s * q \\
 (62) \quad &= r \cdot p' + t(dp' - bq') - s(-cp' + aq') \\
 (63) \quad &= (cs + dt + r)p' - (as + bt)q' \\
 (64) \quad &= t' * p' - s' * q',
 \end{aligned}$$

from which we read off $s' = (as + bt)$ and $t' = (cs + dt + r)$, as desired.

The other cases (negative determinant, and $S = S_{M,r,-}$) are similar.

QED

12. THE SIMILARITY MAPS: PROOF OF CONTINUITY

We show first continuity along the horizontal direction for the similarity maps described Section 10:

Theorem 3. *Given two rational parameters $\theta = p/q, \theta' = p'/q'$, and a correspondence between points in pairs of intervals $I_k, I_{k'}$ in the spectra $\text{Spec}(h_\theta), \text{Spec}(h_{\theta'})$ respectively, given by*

$$(65) \quad x \in I_k \mapsto x' \in I_{k'} = I'_{r \cdot p' + k} \text{ with } (-1)^{q+k} P_\theta(x) = (-1)^{q'+k'} P_{\theta'}(x'),$$

then the correspondence is a continuous bijection on each interval. In particular, this yields a continuous map from the set of points $x \in \text{Spec}(h_\theta)$ into $x' \in \text{Spec}(h_{\theta'})$, with the possible exception at the point $x = 0$, when q is even.

Proof: The polynomial maps $(-1)^{q+k} P_\theta(x), (-1)^{q'+k'} P_{\theta'}(x')$ are both continuous and monotonically increasing on the intervals in question, and thus have continuous inverses. So on each interval, we have a continuous bijection. For q odd, the spectrum $\text{Spec}(h_\theta)$ is a disjoint union of the intervals $I_1 \dots I_q$, and so the collection extends to a continuous map into $\text{Spec}(h_{\theta'})$. In the case where q is even, two of the intervals $I_{q/2}$ and $I_{q/2+1}$ overlap at the point $x = 0$. So, except at this point, the correspondence extends to a continuous map on the union of intervals – that is, it is continuous at $\text{Spec}(h_\theta) \setminus 0$. At the point $x = 0$, the correspondence maps the one point to (possibly) two points, one at the right endpoint of $I'_{r \cdot p' + q/2}$ and the other at the left endpoint of $I'_{r \cdot p' + q/2 + 1}$. This double-valued splitting (although not a singled-valued function) is nevertheless continuous. QED

Figure 16 indicates graphically how the bijection works on level $\theta = 1/3$ to $\theta = 1/5$.

We note that the correspondences of the form

$$(66) \quad x \in I_k \mapsto x' \in I_{k'} = I'_{r \cdot (q' - p') + k} \text{ with } (-1)^{q+k} P_\theta(x) = (-1)^{q'+k'} P_{\theta'}(x'),$$

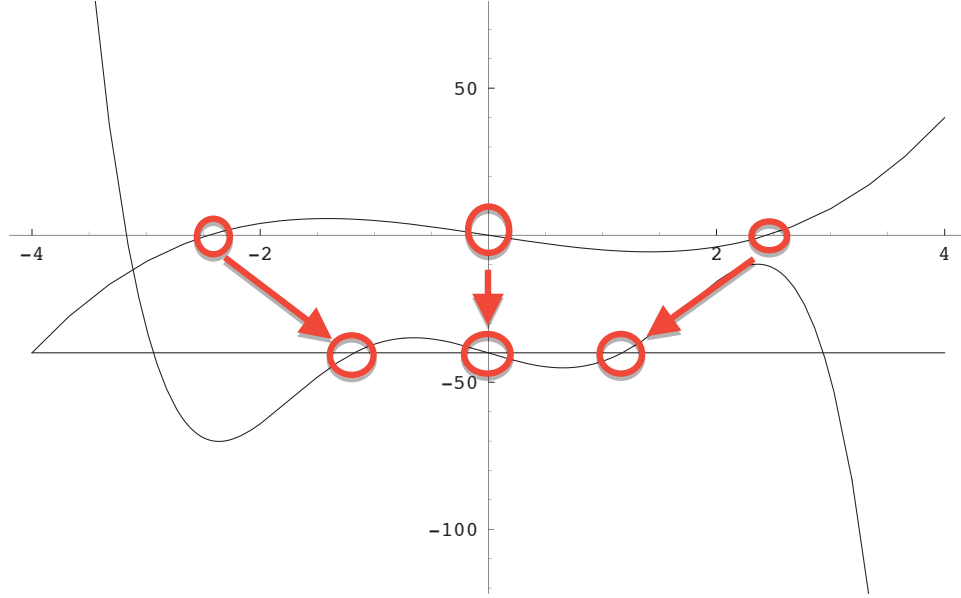


FIGURE 16. Plot of cubic polynomial $P_{1/3}(x)$ and quintic $P_{1/5}(x')$. Match the zero crossing, move polynomials up and down, and observe a continuous correspondence of the zero crossings. This gives the continuous correspondence between line spectra.

also are continuous, as in the theorem. This covers the similarity maps of the form $S_{M,r,-}$.

The numerical work suggests that piecing together these individual polynomial maps, at the different θ levels, gives a continuous map on the whole butterfly. We now state and prove this as a theorem:

Theorem 4. *Suppose $S = S_{M,r,\pm}$ is a similarity of the rational butterfly, as described in Section 10. Then S is a continuous (single-valued) map, except possibly at the points $(x = 0, \theta = p/q)$ with q even, where the map is double-valued and continuous.*

Proof: We consider the case $S = S_{M,r,+}$. Fix a sequence of points (x_n, θ_n) converging to point (x_*, θ_*) and set

$$(67) \quad (x'_n, \theta'_n) = S(x_n, \theta_n).$$

By continuity of the linear fractional transformation, the sequence θ'_n converges to $\theta'_* = (a\theta_* + b)/(c\theta_* + d)$. To show continuity of S , we only need to verify convergence of the x'_n . We will show every convergent subsequence of the image points (x'_n, θ'_n) converges to the point $(x'_*, \theta'_*) = S(x_*, \theta_*)$, which, by compactness, establishes continuity.

Take a convergent subsequence of the (x'_n, θ'_n) with limit (x'_o, θ'_*) . Suppose in this subsequence, there are infinity many points where $\theta'_n = \theta'_*$ (and consequently, $\theta_n = \theta_*$). Applying Theorem 2, by continuity along the spectral lines at θ_* , we can conclude that x'_n converges to x'_* . (Except possibly at $x_* = 0, \theta_* = p/q$, with q even. Here, the map S may be doubly valued, as discussed earlier.)

The other case to consider is when there are at most finitely many n with $\theta'_n = \theta'_*$. By restricting to the tail of the subsequence, and renumbering the subsequence, WLOG we may assume $\theta_n \neq \theta_*$ for all n .

Set the notation consistently, so in the domain we have $\theta_n = p_n/q_n$, $\theta_* = p_*/q_*$, and points $x_n \in I_{k_n}$, $x_* \in I_{k_*}$, while in the range we have $\theta'_n = p'_n/q'_n$, $\theta'_* = p'_*/q'_*$, and points $x'_n \in I'_{k'_n}$, $x'_* \in I'_{k'_*}$, $x'_o \in I'_{k'_o}$. From the definition of S , we know $k'_n = r \cdot p'_n + k_n$ and $k'_* = r \cdot p'_* + k_*$. The value of k'_o is to be determined (it will equal k'_*).

We apply the trace τ_{θ_n} to the spectral projection $\chi_{(-\infty, x_n)}(h_{\theta_n})$. By Lemma 7 in Appendix 2, we have

$$(68) \quad \tau_{\theta_n}(\chi_{(-\infty, x_n)}(h_{\theta_n})) = \frac{k_n - 1}{q_n} + \frac{1}{q_n} F((-1)^{k_n + q_n} P_{\theta_n}(x_n)),$$

where the function F is an integrated density of states on h_o . By continuity of the trace and spectral projection (see (Boca, 2001), Chap. 5), this quantity converges to

$$(69) \quad \tau_{\theta_*}(\chi_{(-\infty, x_*)}(h_{\theta_*})) = \frac{k_* - 1}{q_*} + \frac{1}{q_*} F((-1)^{k_* + q_*} P_{\theta_*}(x_*)).$$

Since the sequence of ratios $p_n/q_n \neq p_*/q_*$ converges to p_*/q_* , we have that q_n converges to infinity, so the terms above with $1/q_n$ in them converge to zero. Thus, from the limit of the traces, we conclude

$$(70) \quad \lim_{n \rightarrow \infty} \frac{k_n}{q_n} = \frac{k_* - 1}{q_*} + \frac{1}{q_*} F((-1)^{k_* + q_*} P_{\theta_*}(x_*)).$$

Similarly, by applying the trace to the sequence of spectral projections on the convergent sequence $x'_n \rightarrow x'_o$, we find

$$(71) \quad \tau_{\theta'_n}(\chi_{(-\infty, x'_n)}(h_{\theta'_n})) = \frac{k'_n - 1}{q'_n} + \frac{1}{q'_n} F((-1)^{k'_n + q'_n} P_{\theta'_n}(x'_n)),$$

converges to

$$(72) \quad \tau_{\theta'_*}(\chi_{(-\infty, x'_o)}(h_{\theta'_*})) = \frac{k'_o - 1}{q'_*} + \frac{1}{q'_*} F((-1)^{k'_o + q'_*} P_{\theta'_*}(x'_o)).$$

Thus

$$(73) \quad \lim_{n \rightarrow \infty} \frac{k'_n}{q'_n} = \frac{k'_o - 1}{q'_*} + \frac{1}{q'_*} F((-1)^{k'_o + q'_*} P_{\theta'_*}(x'_o)).$$

With

$$(74) \quad \frac{k'_n}{q'_n} = \frac{r \cdot p'_n + k_n}{q'_n} = \frac{r \cdot (ap_n/q_n + b) + k_n/q_n}{cp_n/q_n + d}$$

we take limits to obtain the identity

$$(75) \quad \lim \frac{k'_n}{q'_n} = r \cdot \theta'_* + \frac{1}{c\theta_* + d} \lim \frac{k_n}{q_n}.$$

Replacing with the limiting values computed above, we obtain

$$(76) \quad \frac{k'_o - 1}{q'_*} + \frac{1}{q'_*} F((-1)^{k'_o + q'_*} P_{\theta'_*}(x'_o)) = r \cdot \theta'_* + \frac{1}{c\theta_* + d} \left(\frac{k_* - 1}{q_*} + \frac{1}{q_*} F((-1)^{k_* + q_*} P_{\theta_*}(x_*)) \right).$$

Multiplying through by q'_* and simplifying yields

$$(77) \quad k'_o - 1 + F((-1)^{k'_o + q'_*} P_{\theta'_*}(x'_o)) = r \cdot p'_* + k_* - 1 + F((-1)^{k_* + q_*} P_{\theta_*}(x_*)).$$

Now, if x_* is an interior point of the interval I_{k_*} , this last equation has F taking a fractional value strictly between zero and one. Equating the integer part of the equation gives

$$(78) \quad k'_o - 1 = r \cdot p'_* + k_* - 1,$$

from which we conclude $k'_o = k'_*$, which tells us that the limit point x'_o and image point x'_* are in the same spectral interval I'_{k_*} .

Equating the fractional part of the equation gives

$$(79) \quad F((-1)^{k'_o + q'_*} P_{\theta'_*}(x'_o)) = F((-1)^{k_* + q_*} P_{\theta_*}(x_*)),$$

which, from the polynomial correspondence between x_* and x'_* , yields

$$(80) \quad F((-1)^{k'_o + q'_*} P_{\theta'_*}(x'_o)) = F((-1)^{k'_* + q'_*} P_{\theta'_*}(x'_*)).$$

Since F , composed with polynomial $(-1)^{k'_* + q'_*} P_{\theta'_*}(x)$ is strictly increasing on the interval I'_{k_*} , the equality implies $x'_o = x'_*$, as desired.

Now, when x_* is at an endpoint of interval I_k , we use gap labeling to show the limit point x'_o must be the corresponding endpoint of interval I'_{k_*} . Suppose x_* is the left endpoint of interval I_k : in this case, equation 77 reduces to

$$(81) \quad k'_o - 1 + F((-1)^{k'_o + q'_*} P_{\theta'_*}(x'_o)) = r \cdot p'_* + k_* - 1 + 0.$$

so we know that k'_o equals either $k'_* - 1$ or k'_* . We just need to show it is equal to k'_* .

With the point $x_* \neq 0$ at a left endpoint, there must be a gap to the immediate left of x_* , which has some label (s, t) . By continuity of gap labeling (Prop 11.11 in (Boca, 2001)), the gap with this label forms an open set, so for n sufficiently large, the point x_n is to the right of this gap. Hence the interval I_{k_n} is also to the

right of the gap. Since the interval number must be bigger than the gap number, we have

$$(82) \quad k_n > t * p_n - s * q_n.$$

The image point x'_{k_n} is in interval I'_{k_n} and its index satisfies

$$(83) \quad k'_n = r \cdot p'_n + k_n$$

$$(84) \quad > r \cdot p'_n + t * p_n - s * q_n$$

$$(85) \quad = r \cdot p'_n + t * (dp'_n - bq'_n) - s * (-cp'_n + aq'_n)$$

$$(86) \quad = (cs + dt + r) * p'_n - (as + bt) * q'_n$$

$$(87) \quad = t' * p'_n - s' * q'_n$$

where the indices (s', t') label the image gap, as in Theorem 2. Thus the interval $I'_{k'_n}$ is to the right of the gap (s', t') and hence so is the point x'_n . Since this gap is open, the limit point x'_o is to the right of the gap, and thus the interval $I'_{k'_o}$ containing point x'_o is to the right. Consequently, we have

$$(88) \quad k'_o > t'p'_* - s'q'_* = k'_* - 1.$$

This eliminates the possibility that $k'_o = k'_* - 1$, so we are left with $k'_o = k'_*$, from which we quickly conclude that the point x'_o is the left endpoint of interval $I'_{k'_*}$ and thus is equal to x'_* .

Handling a right endpoint is similar. A similar analysis of the case $x_* = 0$ at the common endpoint of two overlapping intervals shows the image sequence x'_n could converge to endpoints of two different, disjoint intervals. QED

It would seem the result on the rational butterfly should extend by continuity to the full butterfly, including irrational values for vertical parameter θ . We state this precisely as a conjecture.

Conjecture 5. *Given a similarity $S = S_{M,r,\pm}$ of the rational butterfly, as described in Section 10, there is a unique continuous extension of S to the full butterfly, possibly double-valued at certain points along the vertical line $x = 0$.*

We do not have a proof of this result. It seems a density argument and use of the continuous trace on the field of rotation algebras A_θ should lead to the result.

It is curious to consider how the polynomial correspondences on the rational spectral lines might extend to irrational values of θ , in which case there are no finite polynomials to describe the mapping.

13. THREE GENERATORS FOR THE BUTTERFLY SIMILARITIES

There are three similarity maps of the butterfly which apparently generate all the similarities discussed above. There is the horizontal flip H defined as the map

$$(89) \quad H(x, \theta) = (-x, \theta).$$

There is the vertical flip V defined as the map

$$(90) \quad V(x, \theta) = (x, 1 - \theta),$$

which can be represented in the form discussed in Section 10 as

$$(91) \quad V = S_{B,0,+},$$

with matrix $B = \begin{bmatrix} -1 & 1 \\ 0 & 1 \end{bmatrix}$. Finally, there is the similarity map discussed in Section 4, taking the butterfly to the bottom half given by

$$(92) \quad S(x, \theta) = (x', \frac{\theta}{\theta + 1}),$$

where $x \in I_k$ in the k -th interval at level θ is mapped to $x' \in I'_k$ in the k -th interval at level θ' . This map is represented as

$$(93) \quad S = S_{A,0,+},$$

for matrix $A = \begin{bmatrix} 1 & 0 \\ 1 & 1 \end{bmatrix}$.

Some elementary calculations show how these three similarities combine algebraically. First, there are the two obvious identities

$$(94) \quad H^2 = I, \quad V^2 = I,$$

and the commutation relation

$$(95) \quad HV = VH.$$

The horizontal flip almost commutes with similarity S ; in fact it just gives a shift in the interval indexing as follows:

$$(96) \quad HS_{A,0,+}H = S_{A,1,+}.$$

This shifting extends to powers of S , so we find

$$(97) \quad (HS_{A,0,+}H)^n = S_{A^n,n,+}.$$

By composing powers of S and HS , we obtain all similarities of the form

$$(98) \quad S_{A^n,r,+} \quad \text{for } 0 \leq r \leq n.$$

We can also verify that such operators combine in the form

$$(99) \quad (S_{A^{n'},r',+})(S_{A^n,r,+}) = S_{A^{n+n'},r+r',+}.$$

The vertical flip does not commute with similarity S , but instead introduces the similarity $S_{M,r,-}$ in the mix. Again, a straightforward calculation shows

$$(100) \quad VS_{A^n,r,+}V = S_{BA^nB,r,-}.$$

As noted in Theorem 1, the matrices A, B generate a large semigroup of linear fractional transformations. From the calculations noted above, the three similarities of the butterfly generate enough similarities to cover this semigroup.

Theorem 6. *The three similarities H, V, S of the rational butterfly generate a semigroup of continuous (possibly double-valued) similarities of the butterfly, including maps of the form*

$$(101) \quad S_{M,r,+} \quad \text{and} \quad S_{M,r,-}$$

where the matrices M range over the semigroup of elements of $GL_2(\mathbb{Z})/\pm I$ representing linear fractional transformations mapping the interval $[0, 1]$ into itself.

The double-valued character is, of course, from the interval splitting in the case of $\theta = p/q$ with q even. There may be other similarities of the butterfly. The point is, we can at least see this large semigroup from $GL_2(\mathbb{Z})$ appearing.

14. CONCLUSIONS

The Hofstadter butterfly, representing spectra of a continuous family of almost Mathieu operators, shows obvious fractal-like symmetry. By investigating these symmetries numerically, we have catalogued the self-similarity maps of the butterfly using a semigroup of Möbius transformations in the vertical direction, indexed by elements in the matrix group $GL_2(\mathbb{Z})$. This semigroup is generated by two matrices. In the horizontal direction, the self-similarity maps are given by algebraic curves determined by characteristic polynomials. Properties of the algebraic curves are demonstrated in a series of plots. These algebraic curves show nearly linear segments, demonstrating an almost linear behaviour in the horizontal component of the self-similarity maps. We proved continuity of the similarity maps on the rational butterfly, possibly double-valued at points with horizontal parameter $x = 0$. The similarity maps are generated by exactly three continuous symmetries. We conjecture the semigroup of similarities on the rational butterfly extends to a family of continuous similarities on the full butterfly.

ACKNOWLEDGMENTS

This work was supported in part by NSERC Discovery grants of the first two authors, and an NSERC Summer Research award of the third author. Numerical calculations were done in MATLAB (TheMathWorks, 2008) and rendered directly

in PostScript, following a method similar to those discussed in (Casselmann, 2005). Algebraic curves were rendered using Mathematica (WolframResearch, 2002).

We would like to thank the organizers of the 2006 BIRS Workshop on Operator Methods in Fractal Analysis, Wavelets, and Dynamical Systems, for encouraging us to present this work in an early form.

REFERENCES

- Arveson, W. 1994. *C*-algebras and numerical linear algebra*, J. Funct. Anal. **122**, no. 2, 333–360.
- Avila, A. and S. Jitomirskaya. 2006. *Solving the ten martini problem*, Lect. Notes. in Physics **690**, 5–16.
- Bellissard, J. 1990. *Gap labelling theorems for Schrödinger operators*, From number theory to physics, pp. 140–150.
- Bellissard, J. and B. Simon. 1982. *Cantor spectrum for the almost Mathieu equation*, Journal of Functional Analysis **48**, no. 3, 408–419.
- Boca, F. 2001. *Rotation c*-algebras and almost Mathieu operators*, Fundatia Theta.
- Brown, E. 1964. *Bloch electrons in a uniform magnetic field*, Phys. Rev. **133**, no. 4A, A1038–A1044.
- Casselmann, B. 2005. *Mathematical Illustrations*, Cambridge University Press.
- Choi, M. D., G. A. Elliott, and N. Yui. 1990. *Gauss polynomials and the rotation algebra*, Invent. Math. **99**, 225–246.
- Connes, A. 1994. *Noncommutative geometry*, Academic Press.
- Coxeter, H.S.M. 1942. *Non-euclidean geometry*, University of Toronto Press, Toronto.
- Effros, E. and C. Shen. 1980. *Approximately finite C*-algebra and continued fractions*, Indiana Univ. Math. J. **12**, no. 2, 191–204.
- Goldman, N. 2009. *Characterizing the Hofstadter butterfly’s outline with Chern numbers*, J. Phys. B: At. Mol. Opt. Phys. **42**, no. 055302.
- Hofstadter, D. R. 1976. *Energy levels and wave functions of Bloch electrons in rational and irrational magnetic fields*, Physical Review B **14**, no. 6, 2239–2249.
- Kaminker, J. and I. Putnam. 2003. *A proof of the gap labeling conjecture*, Michigan Math J. **51**, 537–546.
- Lamoureux, M. P. 1997. *Reflections on the almost Mathieu operator*, Integr. equ. oper. theory **28**, no. 1, 45–59.
- . 2010. *Drawing butterflies from the almost Mathieu operator*. preprint.
- Lamoureux, M. P. and J. A. Mingo. 2007. *On the characteristic polynomial of the almost Mathieu operator*, Proc. AMS **135**, 3205–3215.
- Last, Y. 1994. *Almost everything about the almost Mathieu operator*, Proceedings of the XI-th International Congress of Mathematical physics.
- Mandelbrot, Benoit B. 1990. *The fractal geometry of nature*, Spektrum Akademischer Verlag.
- Puig, Joaquim. 2004. *Cantor spectrum for the almost Mathieu operator*, Comm. in Math Phys **244**, no. 2, 297–309.
- TheMathWorks. 2008. *MATLAB R2008a*.
- WolframResearch. 2002. *Mathematica 4.2*.
- Ypma, F. 2007. *K-theoretic gap labeling for quasicrystals*, Contemporary mathematics: Geometric and topological methods for quantum field theory., pp. 247.

APPENDIX 1

Proof of Theorem 1: We show the corresponding semigroup in $GL(2, \mathbb{Z})/\{\pm I\}$ is generated by the two matrices A and B . Suppose the matrix

$$(102) \quad M = \begin{bmatrix} a & b \\ c & d \end{bmatrix}$$

is in the semigroup. In the case that $b = 0$, the determinant condition gives $a = \pm d = \pm 1$; the condition that the LFT maps $[0, 1]$ into $[0, 1]$ reduces WLOG to $a = d = 1$ and $c \geq 0$. This leave matrix M in the form

$$(103) \quad M = \begin{bmatrix} 1 & 0 \\ c & 1 \end{bmatrix} = A^c,$$

with $c \geq 0$. Hence the matrix M is generated by A alone.

In the case that $b \neq 0$, WLOG (by mod-ing out by $\pm I$), we can assume $d \geq b > 0$ as we know that 0 maps to $b/d \in [0, 1]$ under the LFT. By the determinant condition $ad - bc = \pm 1$, we have that the gcd of b, d is one, so we may apply the Euclidean algorithm to obtain a sequence of strictly positive quotients q_0, q_1, q_2, \dots and remainders $b = r_0, r_1, r_2, \dots$ with

$$\begin{aligned} d &= q_0 r_0 + r_1 \\ b &= q_1 r_1 + r_2 \\ r_1 &= q_2 r_2 + r_3 \\ &\dots \\ r_{k-1} &= q_k r_k + r_{k+1}, \end{aligned}$$

where $r_k = \gcd(b, d) = 1$ and $r_{k+1} = 0$. Applying these values to matrix M , we can factor as

$$\begin{aligned} \begin{bmatrix} a & b \\ c & d \end{bmatrix} &= \begin{bmatrix} 0 & 1 \\ 1 & q_0 \end{bmatrix} \begin{bmatrix} a_0 & r_1 \\ c_0 & r_0 \end{bmatrix} \\ &= \begin{bmatrix} 0 & 1 \\ 1 & q_0 \end{bmatrix} \begin{bmatrix} 0 & 1 \\ 1 & q_1 \end{bmatrix} \begin{bmatrix} a_1 & r_2 \\ c_1 & r_1 \end{bmatrix} \\ &= \begin{bmatrix} 0 & 1 \\ 1 & q_0 \end{bmatrix} \begin{bmatrix} 0 & 1 \\ 1 & q_1 \end{bmatrix} \cdots \begin{bmatrix} 0 & 1 \\ 1 & q_k \end{bmatrix} \begin{bmatrix} a_k & 0 \\ c_k & 1 \end{bmatrix}, \end{aligned}$$

for some appropriate values of $a_0, a_1, \dots, c_0, c_1, \dots$

Now, the matrix factors with the q_j are generated by the A, B matrices, since

$$(104) \quad \begin{bmatrix} 0 & 1 \\ 1 & q \end{bmatrix} = A^{q-1} B A.$$

In the last factor,

$$(105) \quad \begin{bmatrix} a_k & 0 \\ c_k & 1 \end{bmatrix},$$

we know that c_k is non-negative, else the LFT has a pole in $[0, 1]$, which is not allowed. By the determinant condition, we have $a_k = \pm 1$. In the case $a_k = 1$, we have that the last factor appears as

$$(106) \quad \begin{bmatrix} 1 & 0 \\ c_k & 1 \end{bmatrix} = A^{c_k}.$$

In the case where $a_k = -1$, we may combine the last two factors to observe

$$\begin{aligned} \begin{bmatrix} 0 & 1 \\ 1 & q \end{bmatrix} \begin{bmatrix} -1 & 0 \\ c & 1 \end{bmatrix} &= \begin{bmatrix} 0 & 1 \\ 1 & q \end{bmatrix} \begin{bmatrix} 1 & -1 \\ 0 & 1 \end{bmatrix} \begin{bmatrix} c-1 & 1 \\ c & 1 \end{bmatrix} \\ &= \begin{bmatrix} 0 & 1 \\ 1 & q-1 \end{bmatrix} \begin{bmatrix} c-1 & 1 \\ c & 1 \end{bmatrix} \\ &= (A^{q-2}BA)(BA^c). \end{aligned}$$

For $q \geq 2$, we are done: these last factors appear as generated by matrices A, B , as desired.

In the case $q = 1$, it easy to check that we must have more than one q -type matrix in the factorization, for if not, we get

$$(107) \quad \begin{bmatrix} a & b \\ c & d \end{bmatrix} = \begin{bmatrix} 0 & 1 \\ 1 & q_0 \end{bmatrix} \begin{bmatrix} -1 & 0 \\ c_0 & 1 \end{bmatrix},$$

where $q_0 = 1$, giving an LFT mapping 1 to $(c+1)/c$, which is outside the interval $[0, 1]$. With a second q -type matrix in the factorization, we get

$$(108) \quad M = \cdots (A^{q-1}BA)(A^{-1}BA)(BA^{c_k}) = \cdots (A^{q-1}B)(AA^{-1})(BA)(BA^{c_k}) = \cdots A^qBA^{c_k},$$

which puts M in the semigroup generated by A, B . QED

Here is a nice example, to show that the $a_k = -1$ case really does appear.

$$(109) \quad \begin{bmatrix} 2 & 1 \\ 3 & 2 \end{bmatrix} = \begin{bmatrix} 0 & 1 \\ 1 & 2 \end{bmatrix} \begin{bmatrix} -1 & 0 \\ 2 & 1 \end{bmatrix}$$

The matrix on the left gives an LFT which maps 0 to $1/2$, and 1 to $3/5$. This similarity map actually appears in the Hofstadter butterfly, as we can see by examining Figure 1. We get $a_1 = -1$ in the factorization, which perhaps was not expected. Thus that little factor matrix on the right is not in the semigroup, since it maps 1 to $-1/3$, and thus does not map interval $[0, 1]$ to itself.

However, the original matrix on the left is actually in the semigroup, as shown in the proof.

APPENDIX 2

We prove a basic result concerning the trace of certain spectral projections in the rotation algebra A_θ . The machinery for this result is standard, and we borrow heavily from the results in (Boca, 2001).

Lemma 7. *Let τ_θ and τ_o be the (framed) tracial states on rotation algebras A_θ, A_o , respectively, with $\theta = p/q$. Let $[a, b]$ be the k -th interval I_k in the spectrum of the operator $h_\theta = u + u^* + v + v^*$ in algebra A_θ . Then for $x \in [a, b]$,*

$$(110) \quad \tau_\theta(\chi_{[a,x]}(h_\theta)) = \frac{1}{q} \tau_o(\chi_{[-4,(-1)^{k+q}P_\theta(x)]}(h_o)),$$

where $\chi_{[a,x]}$ is the spectral projection onto interval $[a, x]$. Consequently,

$$(111) \quad \tau_\theta(\chi_{(-\infty,x]}(h_\theta)) = \frac{k-1}{q} + \frac{1}{q} \tau_o(\chi_{[-4,(-1)^{k+q}P_\theta(x)]}(h_o)).$$

Note: the choice of the sign in front of polynomial $P_\theta(x)$ ensures that the map

$$(112) \quad x \mapsto (-1)^{k+q}P_\theta(x)$$

is monotonic *increasing* on the interval I_k . In the earlier sections of this paper, it is convenient to write the trace-spectral projection function as the cumulative density $F(x)$ for the operator h_o , so we may write

$$(113) \quad \tau_\theta(\chi_{(-\infty,x]}(h_\theta)) = \frac{k-1}{q} + \frac{1}{q} F((-1)^{k+q}P_\theta(x)),$$

where

$$(114) \quad F(x) = \tau_o(\chi_{[-4,x]}(h_o))$$

is a continuous, strictly increasing function mapping $[-4, 4]$ onto $[0, 1]$.

Proof: We do a direct calculation. The trace on A_θ is obtained from a representation of the algebra in $C(\mathbb{T}^2) \otimes M_q(\mathbb{C})$ with generators

$$(115) \quad u = \iota_1 \otimes U_o, v = \iota_2 \otimes V_o,$$

where the functions ι_1, ι_2 are the coordinate maps $\iota_1(z_1, z_2) = z_1, \iota_2(z_1, z_2) = z_2$, and the $q \times q$ matrices U_o, V_o are the usual cyclic permutation and the diagonal with powers of $e^{2\pi i \theta}$. The trace in this frame is just

$$(116) \quad \tau_\theta = \mu_2 \otimes tr_q,$$

where μ_2 is the usual Haar measure on \mathbb{T}^2 and tr_q is the normalized trace on $q \times q$ matrices. (See (Boca, 2001), page 11.)

Fix x in I_k . The matrix-valued function $h = u + u^* + v + v^*$ has exactly one eigenvalue in the interval I_k , which moves continuously for parameter values $(z_1, z_2) \in \mathbb{T}^2$. This eigenvalue contributes to the trace precisely when it lies in the interval $[a, x]$. That is, we get a contribution precisely when the value of the polynomial $(-1)^{k+q}P_\theta(x)$ is smaller than $z_1^q + \bar{z}_1^q + z_2^q + \bar{z}_2^q$. We compute the trace in terms of a characteristic function on the torus \mathbb{T}^2 , normalized by q , so

$$(117) \quad \tau_\theta(\chi_{[a,x]}(h_\theta)) = \frac{1}{q} \int_{\mathbb{T}^2} \chi_{((-1)^{k+q}P_\theta(x) < z_1^q + \bar{z}_1^q + z_2^q + \bar{z}_2^q)} d\mu_2.$$

With $y = (-1)^{k+q}P_\theta(x)$, and noting that the map $(z_1, z_2) \mapsto (z_1^q, z_2^q)$ has measure preserving inverse on the torus, we can write

$$\begin{aligned} \tau_\theta(\chi_{[a,x]}(h_\theta)) &= \frac{1}{q} \int_{\mathbb{T}^2} \chi_{(y < z_1^q + \bar{z}_1^q + z_2^q + \bar{z}_2^q)} d\mu_2 \\ &= \frac{1}{q} \int_{\mathbb{T}^2} \chi_{(y < z_1 + \bar{z}_1 + z_2 + \bar{z}_2)} d\mu_2 \\ &= \frac{1}{q} \int_{\mathbb{T}^2} \chi_{(P_o(y) < z_1 + \bar{z}_1 + z_2 + \bar{z}_2)} d\mu_2 \\ &= \frac{1}{q} \tau_o(\chi_{[-4,y]}(h_o)). \end{aligned}$$

where we use the fact that $P_o(y) = y$ and so the last integral above yields the trace in A_o applied to the spectral projection obtained by applying $\chi_{[-4,y]}$ onto h_o .

Using the relation $y = (-1)^{k+q}P_\theta(x)$, we obtain

$$(118) \quad \tau_\theta(\chi_{[a,x]}(h_\theta)) = \frac{1}{q} \tau_o(\chi_{[-4,(-1)^{k+q}P_\theta(x)]}(h_o)),$$

as desired. The trace evaluated on the full interval $(-\infty, x)$ picks up an additional contribution of $(k-1)/q$ from the previous $k-1$ intervals in the spectrum. QED

It is worth noting that this trace integral can be computed explicitly, the result involves an integral of $\arccos(y/2 + \cos(\theta))$.

APPENDIX 3

We conclude with some final plots of the algebraic curves which determine the horizontal component of the similarity maps. Properties to notice are that the curves have even symmetry for denominator q even, odd symmetry for q odd, and in all cases there is a sequence of nearly linear segments along the diagonal line $y = x$. It

is also notably that as the numerator p increases, the algebraic curves become much more complicated.

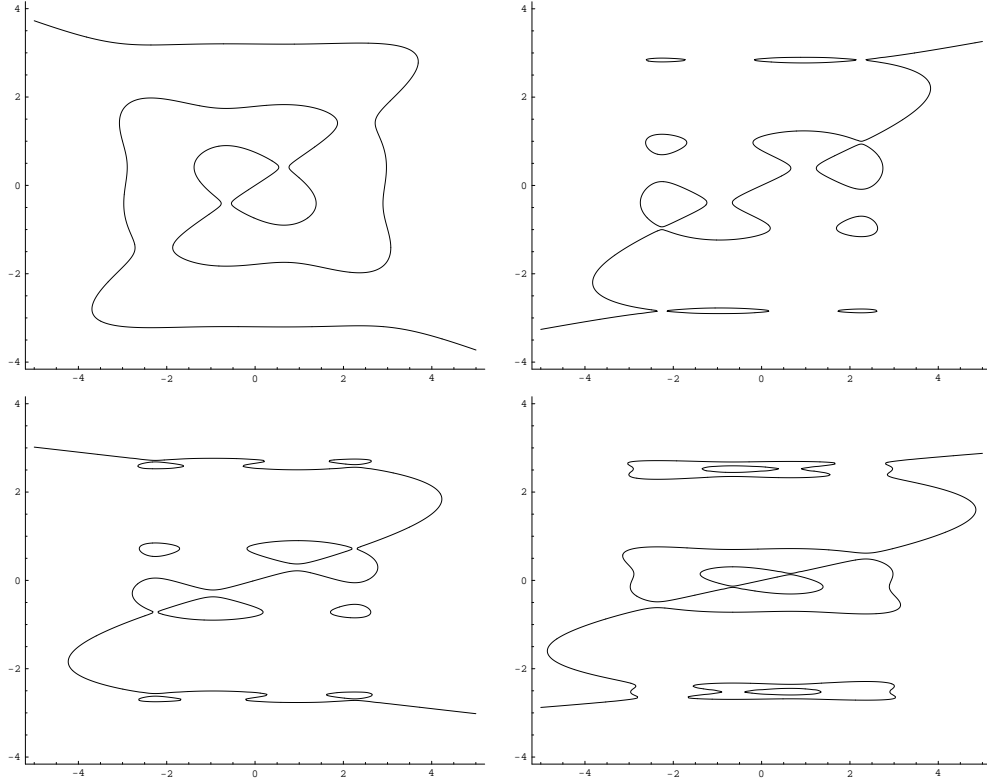


FIGURE 17. Algebraic curves with denominator 5: $1/5 \mapsto 1/7$, $2/5 \mapsto 2/9$, $3/5 \mapsto 3/11$, $4/5 \mapsto 4/13$. In each graph, there are five nearly linear segments down the diagonal of the graph. All but the first graph have some disconnected components.

..

..

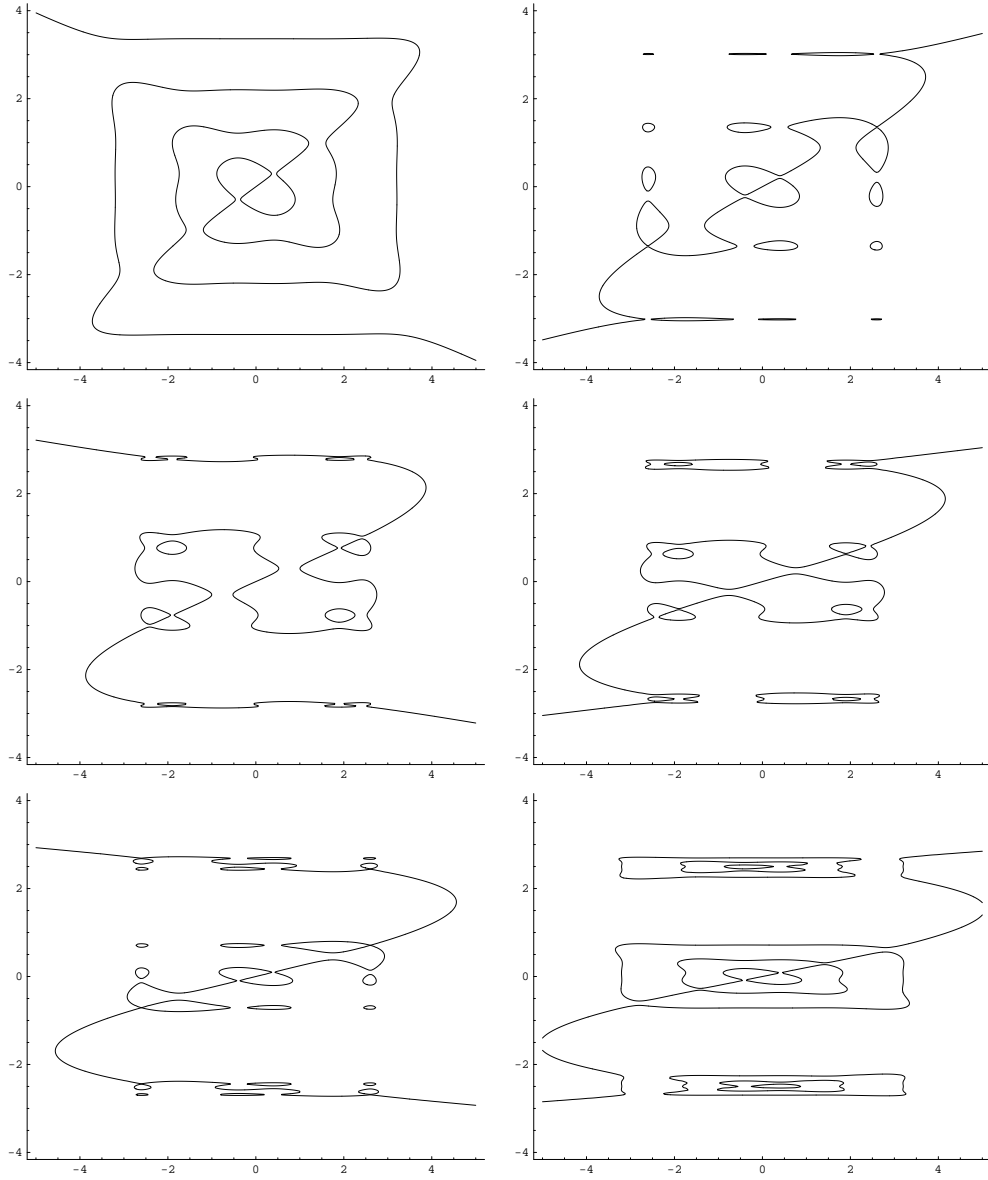


FIGURE 18. Algebraic curves with denominator 7: $1/7 \mapsto 1/9$, $2/7 \mapsto 2/11$, $3/7 \mapsto 3/13$, $4/7 \mapsto 4/15$, $5/7 \mapsto 5/17$, $6/7 \mapsto 4/19$. In each graph, there are seven nearly linear segments down the diagonal of the graph. All but the first graph have some disconnected components.

..

..

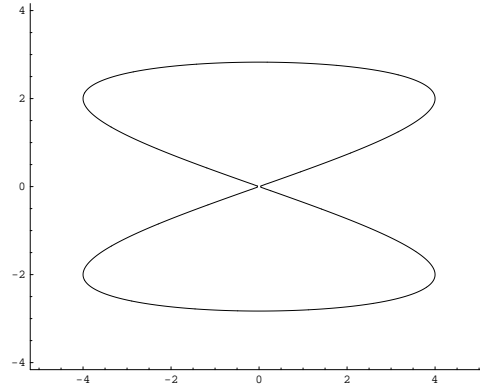


FIGURE 19. Algebraic curve with denominator 2, the $1/2 \mapsto 1/4$ map.

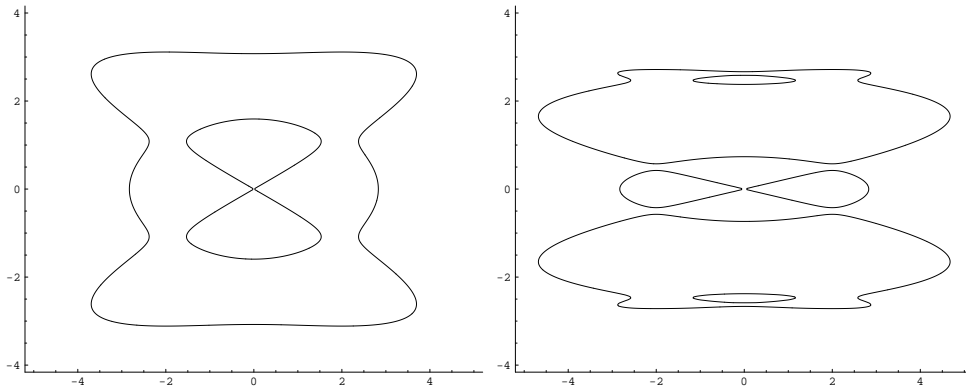


FIGURE 20. Algebraic curves with denominator 4: $1/4 \mapsto 1/6$, $3/4 \mapsto 3/10$. In each graph, there are four nearly linear segments down the diagonal of the graph. The right graph has some components which are disconnected from the linear segments.

..

..

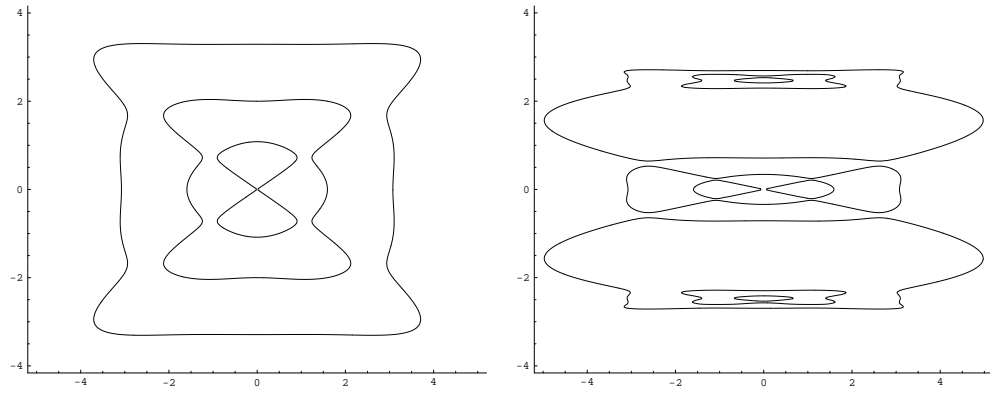


FIGURE 21. Algebraic curves with denominator 6: $1/6 \mapsto 1/8$, $5/6 \mapsto 5/16$. In each graph, there are six nearly linear segments down the diagonal of the graph. The right graph has some components which are disconnected from the linear segments.

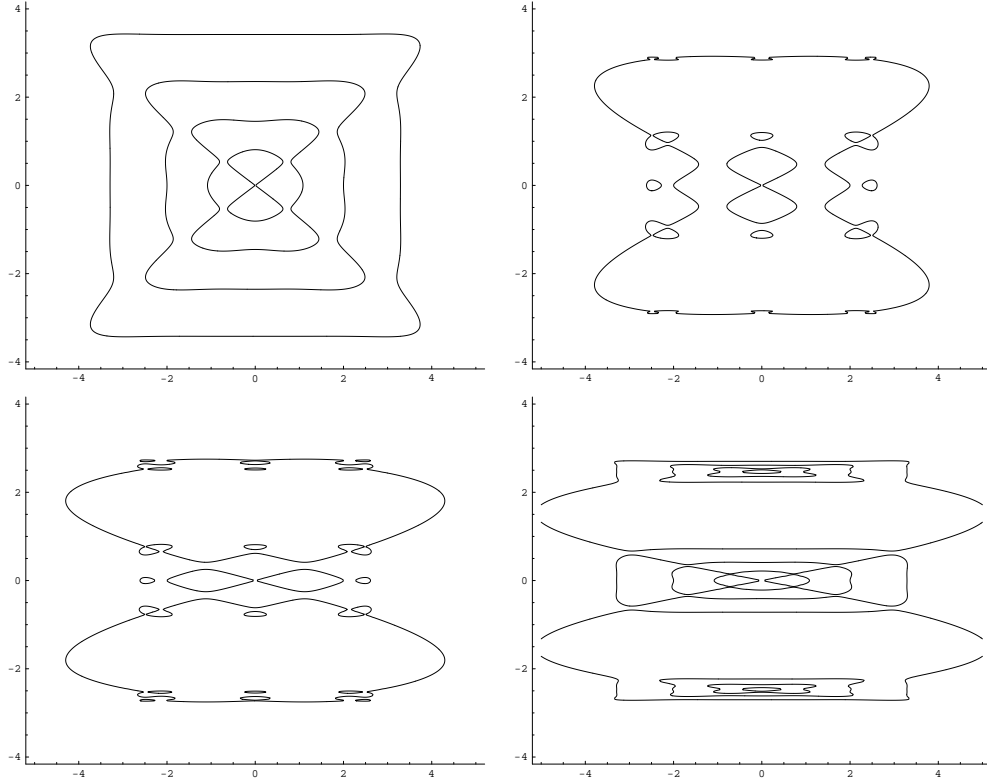


FIGURE 22. Algebraic curves with denominator 8: $1/8 \mapsto 1/10$, $3/8 \mapsto 3/14$, $5/8 \mapsto 5/18$, $7/8 \mapsto 7/22$. In each graph, there are eight nearly linear segments down the diagonal of the graph. All but the first graph has some components which are disconnected from the linear segments.

(M. Lamoureux) DEPT. MATHEMATICS AND STATISTICS, UNIVERSITY OF CALGARY, 2500 UNIVERSITY AVE NW, CALGARY AB T2N 1N4, CANADA

E-mail address: mikel@math.ucalgary.ca

(J. Mingo) DEPT. MATHEMATICS AND STATISTICS, QUEENS UNIVERSITY, KINGSTON, ON CANADA

E-mail address: mingo@mast.queensu.ca

(S. Pachmann) FACULTY OF ENGINEERING, UNIVERSITY OF CALGARY, CALGARY AB, CANADA

E-mail address: sydney.pachmann@gmail.com